This is a repository copy of *Preservation of titanosaur egg clutches in Upper Cretaceous cumulative palaeosols (Los Llanos Formation, La Rioja, Argentina)*.

White Rose Research Online URL for this paper:
http://eprints.whiterose.ac.uk/117262/

Version: Accepted Version

## Article:

# Accepted Manuscript

Preservation of titanosaur egg clutches in Upper Cretaceous cumulative palaeosols (Los Llanos Formation, La Rioja, Argentina)

Giorgio Basilici, Esteban Martín Hechenleitner, Lucas Ernesto Fiorelli, Patrick Führ Dal Bó, Nigel Philip Mountney
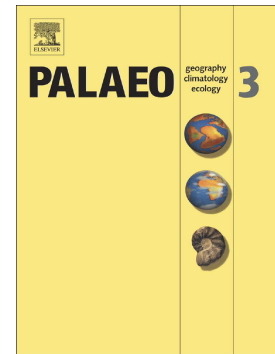
Please cite this article as: Giorgio Basilici, Esteban Martín Hechenleitner, Lucas Ernesto Fiorelli, Patrick Führ Dal Bó, Nigel Philip Mountney , Preservation of titanosaur egg clutches in Upper Cretaceous cumulative palaeosols (Los Llanos Formation, La Rioja, Argentina), *Palaeogeography, Palaeoclimatology, Palaeoecology* (2017), doi: 10.1016/j.palaeo.2017.05.034

PRESERVATION OF TITANOSAUR EGG CLUTCHES IN UPPER CRETACEOUS CUMULATIVE PALAEOSOLS (LOS LLANOS FORMATION, LA RIOJA, ARGENTINA)

Running Head: Titanosaur egg-clutches in cumulative palaeosols

Giorgio Basilici[1,2], Esteban Martín Hechenleitner[2], Lucas Ernesto Fiorelli[2], Patrick Führ Dal Bó[3], Nigel Philip Mountney[4]

[1] Department of Geology and Natural Resources, Institute of Geosciences, State University of Campinas, 13083-870, Campinas (SP), Brazil.

[2] Centro Regional de Investigaciones Científicas y Transferencia Tecnológica de La Rioja (CRILAR-CONICET), Provincia de La Rioja, UNLaR, SEGEMAR, UNCa, CONICET, Entre Ríos y Mendoza s/n., 5301, Anillaco, La Rioja, Argentina.

[3] Department of Geology, Institute of Geosciences, Federal University of Rio de Janeiro, Rio de Janeiro (RJ), Brazil.

[4] Fluvial & Eolian Research Group, School of Earth and Environment, University of Leeds, Leeds, LS2 9JT, UK.

ABSTRACT

Studies of the palaeobiology of titanosaur eggs are significantly more common than studies of titanosaur-egg-bearing strata. Nevertheless, the latter provide significant insight into palaeoenvironmental conditions associated with the egg-laying behaviour. This study examines titanosaur-egg-bearing strata of the Upper Cretaceous Los Llanos Formation (La Rioja, Argentina) and relates them to the laying and preservation of titanosaur egg clutches. Los Llanos Formation is a predominantly sandstone succession throughout represented by palaeosol profiles. Five titanosaur egg clutches were recovered from the Bw horizon of an Inceptisol profile. This palaeosol type, named

Tama pedotype, constitutes 69% of the entire succession, by thickness. Rare planar, and undulating lamination and cross stratification, quartz-grain surface microtextures and ventifacts are indicative of the interaction of fluvial-aeolian processes of sedimentation during accumulation of the parent material on the distal part of a coalescent alluvial fan system (*bajada*). Highly abundant root traces, reddish colour, clay coatings and calcium carbonate nodules testify that the Tama pedotype had abundant vegetation cover, and was developed in well-drained conditions under the influence of a semiarid climate regime. Palaeosol horizons with exaggerated thickness and diffuse boundaries indicate a cumulative pedotype, whereby the soil developed in response to continuous accretion via on-going sedimentary processes.

Morphological features of eggshells suggest that titanosaurs dug holes in the topographic surface to lay eggs. Thus, palaeosols seem to have been putative areas for the laying of titanosaur eggs. Actually, it is uncommon for palaeosols to constitute sites for the preservation of eggs, since soils typically develop in response to long episodes of weathering. However, cumulative palaeosols can provide ideal conditions for egg burial and preservation. In cumulative soils, the residence time of an object within the weatherable thickness of a soil is reduced to less than $10^3$ years, thereby significantly increasing the long-term preservation potential of eggs.

**Key words**: Titanosaur egg clutches; Cumulative palaeosols; Semiarid palaeoenvironment; Late Cretaceous; Los Llanos Formation; La Rioja - Argentina.

1. INTRODUCTION

Studies providing details of the taxonomy, palaeobiology and palaeoecology of titanosaur eggs and nesting sites are numerous (e.g., Carpenter et al., 1994; Hirsch, 2001; Chiappe et al., 2004; 2005; Grellet-Tinner et al., 2006; Salgado et al., 2009; Grigorescu et al., 2010; Vila et al., 2010; Fiorelli et

al., 2012; García et al., 2015; Hechenleitner et al., 2015, 2016). By contrast, studies focused on palaeoenvironmental aspects of titanosaur egg-bearing strata are not common (for a synthesis see Paik et al., 2012). These studies indicate that egg-bearing strata are dominantly represented by fluvial floodplain, distal alluvial-fan, coastal and inland interdune palaeoenvironments (Tandon et al., 1995; López-Martínez et al., 2000; Chiappe et al., 2004; Díaz-Molina et al., 2007; Saneyoshi et al., 2008; Kim et al., 2009; Liang et al., 2009; Paik et al. 2012; García et al., 2015; Hechenleitner et al., 2016). In some sedimentary successions where *in situ* eggs have been found, some described aspects of the egg-bearing strata are indicative of palaeosols: the concentration of calcareous nodules, the presence of mottles, rhizoliths, bioturbation, a red-brown colour, and the general absence of primary sedimentary structures (Tandon et al., 1995; López-Martínez et al., 2000; Kim et al., 2009; Hechenleitner et al., 2016). Actually, some articles describe titanosaur eggs preserved in palaeosols (Sander et al., 1998; Van Itterbeek et al., 2004; 2005; Paik et al., 2004; Bojar et al., 2005), though very few articles consider the aspects of such palaeosols in detail (Cojan et al., 2003). In other cases, where palaeosol profiles contain titanosaur eggs, authors have asserted that the eggs were buried by sedimentary processes and that the pedogenesis occurred later (Liang et al., 2009; Grigorescu et al., 2010).

This article seeks to resolve four general research questions: (i) Are titanosaur-egg-bearing strata commonly associated with palaeosols? (ii) Was the pedogenesis later than or contemporaneous to the egg laying? (iii) What conditions allowed the laying and the preservation of eggs of titanosaurs in palaeosols? (iv) What palaeosol types are most likely associated to the preservation of eggs of titanosaurs?

Los Llanos Formation, which is exposed near the locality of Tama (La Rioja, Argentina) (Fig. 1), is an Upper Cretaceous sandstone unit where palaeosol profiles occur throughout the succession. *In situ* egg clutches of titanosaurs were found in this formation (Fig. 2) for which it is possible study and

reconstruct the paleoenvironmental conditions that allowed the laying of the eggs and their preservation into the sedimentary record.

With the goal of contributing to the understanding of titanosaur nesting palaeontological sites, this study (i) interprets the palaeoenvironmental conditions that enable the generation of the palaeosols that contain the titanosaur eggs, and (ii) examines the circumstances that permitted the preservation of egg clutches within the palaeosols. Results help to clarify the preferred palaeoenvironmental conditions that titanosaurs selected to lay eggs, and which influenced their preservation into the geological record.

## 2. GEOLOGICAL AND STRATIGRAPHIC SETTING

Los Llanos Formation is exposed in small outcrops (2-20 $km^2$) in the central-east region of La Rioja province, Western Argentina (Fig. 1). However, seismic and drilling data indicate a larger spatial extent beneath Quaternary deposits and a thickness up to 290 m (Fisher et al., 2002; Vujovich et al., 2007). The study area is located southwest of the small town of Tama (Fig. 1). Here, Los Llanos Formation crops out as a *c.* 70 m-thick succession (Fig. 2). The base of this unit is characterised by a near-flat but erosional surface. Along a 3 km-long, north-south oriented transect this basal surface caps two stratigraphic units: (i) a cross-stratified and planar-laminated sandstone (the Carboniferous-to-Permian Patquía Formation); (ii) an Ordovician leucogranite. In this area Los Llanos Formation dips 3° towards the WNW and is unconformably overlain by a horizontally bedded, Neogene or Quaternary coarse-grained sandstone and conglomerate (Fig. 2). Los Llanos Formation contains freshwater ostracods and charophytes (Carignano et al., 2013), articulated remains of the three dinosaur clades (ornithischians, sauropods and theropods) (Hechenleitner et al., 2014), turtles, notosuchian crocodyliforms (Fiorelli et al., 2016) and titanosaur eggs preserved *in situ* (Hechenleitner et al., 2016). Collectively, the palaeontological record indicates an Upper Cretaceous age for this unit.

At the studied locality, deposits of Los Llanos Formation are characterised dominantly (79% of succession) by pale reddish orange, moderately sorted, medium- and fine-grained sandstone with less than 2% granule and small pebble clasts (Fig. 2). Additionally, pebbly sandstone and muddy sandstone also occur (14 and 7% of succession, respectively). Beds with high calcium carbonate content are particularly common in the lower part of the succession. Primary sedimentary structures are near absent: only in few places are sets of faint traces of medium-scale cross-stratification and planar lamination observed. Within the structureless sandstone deposits, rhizoliths, carbonate nodules and mottles are all abundant (Fig. 2); these features indicate the presence of numerous vertically stacked palaeosol profiles. Previous detailed sedimentological and stratigraphic studies of Los Llanos Formation interpreted this sedimentary succession to be of braided alluvial origin, characterised by intense pedogenesis (Ezpeleta et al., 2006).

3. METHODS

We measured a stratigraphic log of all the exposed section of Los Llanos Formation in an area of 12 km$^2$ to the southwest of the town of Tama (Figs 1 and 2). Palaeosol profiles dominate throughout the entire sedimentary succession; few primary sedimentary structures are preserved. Exposure conditions permitted detail examination of *c.* 65% of the succession. In the field, palaeosols were distinguished according to the following characteristics: presence and distribution of root traces, colour, abundance and size of calcareous nodules, style of mottle development and type of horizon development. Field estimations of abundance of calcium carbonate and boundary distinctness, and topography of the palaeosol horizons were made using the recommendations of Retallack (2001) and Schoeneberger et al. (2012). The deposits were differentiated based on the presence of sedimentary structures. Twenty-seven palaeosol profiles were examined and recorded in the detailed logs. These were divided into two pedotypes (Retallack, 1994): Tama and Colozacán pedotypes. The Tama

pedotype is the one that contains the egg clutches and is therefore described in more detail herein than the Colozacán pedotype. Compositional features of clasts more than 20 mm across were determined in the field on 1 $m^2$ exposed surfaces of three pebbly sandstone beds. Thirty-two fresh sandstone samples of palaeosol profiles were collected from different portions of the succession (see Fig. 2) for laboratory geochemical and micromorphological analyses. Major oxides and trace elements of fused beads and pressed pellets, respectively, were determined in 21 samples by X-ray fluorescence spectrometer (Philips, PW2404). Thirty-two thin sections of palaeosol were made for micromorphological analyses. Textural and petrographic features of sandstone were defined in 12 thin sections by counting more than 300 points in each. Classification schemes of the USDA (Soil Survey Staff, 1999) and Mack et al. (1993) were used to classify the palaeosols.

Fifteen quartz grains in the size range of 600 to 1100 $\mu$m were randomly picked after washing and sieving from two samples of palaeosols (cf. Vos et al., 2014): one collected at the site of the egg clutch discoveries and the latter in a typical Tama pedotype located at the 25 m level of the measured section (Fig. 2). Using a scanning electron microscope (SEM - mod. LEO 430) in secondary electron imaging mode, we described the surface microtextures for each grain to define the mechanisms of transport and sedimentation of the parent material. Name and microtexture definitions have been adopted by Mahaney (2002) and Vos et al. (2014).

4. DEPOSITS AND DEPOSITIONAL PALAEOENVIRONMENT

Based on analysis of textural features, three lithofacies are distinguished in the studied succession of Los Llanos Formation: sandstone, pebbly sandstone and muddy sandstone.

4.1. Sandstone

Medium- and fine-grained sandstone (Fig. 3A and Tab. 1) represents 79% of the thickness of the measured succession. This sandstone is classified as a feldspathic litharenite (Pettijohn et al., 1987) (Fig. 3B and Tab. 1). In general, sedimentary structures and original bounding surfaces of the beds are absent. Only in a small number of cases (<2% of the total succession) are weakly preserved planar, undulating and parallel laminations evident in beds up to 0.2 m thick (Fig. 3C and Tab. 1).

The frequency distribution of 20 specific quartz grain microtextures of two samples from the site of the egg clutch discovery and at the 25 m level of the measured section (Fig. 2) is shown in Fig. 4. The main microtextures observed, in decreasing order of frequency distribution, are: low relief, upturned plates, rounded grain outlines, adhering particles, bulbous edges and edge rounding, v-shaped percussion cracks and conchoidal fractures. Most of the quartz grains have low relief, i.e. a smooth surface that lacks significant local irregularity (Fig. 5A and C). Upturned plates are one of the most representative microtextures of the quartz grains (Margolis and Krinsley, 1971) (Fig. 5B, D, E and F). Rounded outlines are a characteristic of 67-80% of the quartz grains (Fig. 5A and C); the remaining ones are subrounded. Adhering particles, consisting of micrometric silica fragments, occur scattered on grain surfaces (Fig. 5A, B and E). Bulbous edges and edge rounding (Fig. 5A and C) are two common and related features (Mahaney, 2002). Bulbous edges are commonly associated with elongated or equidimensional depressions (Fig. 5A). V-shaped percussion cracks, although not numerous on the surfaces of individual grains, are present on more than 50% of clasts (Fig. 5B, D and E). Conchoidal fractures are also present (Fig. 5C and F). Some quartz grains show overprinted generations of different microtextures (Fig. 5B, D, E and F); for example in figure 5F, a conchoidal fracture is covered and altered by smaller upturned plates. Less representative microtextures are: arcuate and straight steps (Fig. 5F), graded arcs,  and solution pits (Fig. 5D).

*Interpretation*. The limited thickness, the absence of any evident internal grain-size trend, the absence of a pronounced grain-size differentiation and of sets separated by distinct bounding

surfaces suggest that the planar, undulating and parallel laminations have a subaqueous origin, developed in upper flow regime conditions (Harms et al., 1975; Cheel and Middleton, 1986; Fielding, 2006).

The diagram of frequency distribution (Fig. 4) shows that most of the microtextures – and in particular those with frequency distribution >50% – have very similar values in the two samples, indicating that the quartz grains were subjected to similar transport processes. Microtextures of quartz grains can be interpreted as follows. Low relief is a peculiar feature of grains transported by aeolian processes (Vos et al., 2014; see their Tab.2). Upturned plates are very typical of grains of aeolian origin (Vos et al., 2014) formed from ballistic collisions that cause the shattering of the cleavage planes of the quartz (Margolis and Krinsley, 1974; Krinsley et al., 1976). Pronounced rounding of quartz grains occurs readily during aeolian grain saltation. However, rounded and subrounded grains can also form in upper flow regime in subaqueous flows of fluvial environments (Madhavaraju et al., 2009). Silica adhering particles may be associated with abrasion fatigue of grain surfaces in an aeolian environment that favours the attachment of small fragments to grain surfaces (Mahaney, 2002). The rounding and prominent shape of bulbous edges is attributed to the rotation of grains during saltation arising from aeolian transport (Costa et al., 2013). Edge rounding commonly occurs in wind-blown grains (Mahaney, 2002). V-shaped percussion cracks correspond to the effect of casual collision between grains and are typical of highly energetic fluvial transport (Margolis and Krinsley, 1974). Conchoidal fractures are formed as consequence of powerful impact on grain surface. These microtextures, with dimension >50 $\mu$m, as in these samples, are common in subaqueous flows where pebbles hit smaller grains (Vos et al., 2014); they are larger than those typically developed in response to aeolian grain saltation. Arcuate and straight steps, which are associated with conchoidal fractures, have the same origin. Graded arcs are produced by impact with other grains in aeolian and

subaqueous environments. Solution pits are due to the dissolution of the silica during pedogenesis or diagenesis (Vos et al., 2014).

### 4.2. Pebbly sandstone

Pebbly sandstone represents 14% of the thickness of the measured succession (Tab. 1). Beds of this lithofacies are common in the lower part of the succession. This lithofacies is characterised by poorly sorted, medium to coarse-grained sand with granule to boulder clasts. Several of the examined clasts, from small pebble- to boulder-size, possess notable pyramidal shapes, characterised by flattened facets and well-developed crests (Fig. 6A) in a form that is common to ventifacts (Laity, 1994). This lithofacies is represented by tabular beds with erosive bottom and poorly preserved trough cross-stratified sets (Fig. 6B); trough axes reveal a palaeotransport direction towards the WNW (Fig. 6C).

*Interpretation*. The generally coarse grain-size, the trough cross-bedding and the erosive bases of the pebbly sandstone beds demonstrates hydraulic transport and deposition (Bridge, 2003). The large ratio of width-to-thickness of these beds, and the great extent of the tabular bodies indicates sediment transport and deposition in non- or poorly channelised subaqueous flows, probably characterised by a high and ephemeral hydraulic regime, as supported by the poorly sorted sediments (Nichols and Fisher, 2007; Banham and Mountney, 2014). Palaeocurrent data reveal flows from the ESE.

### 4.3. Muddy sandstone

Muddy sandstone represents 7% of the thickness of the measured succession. This lithofacies is characterised by structureless, muddy sand (Fig. 6D and Tab.1). Only two lenticular beds up to 4 m

thick and with sharp boundaries were observed (Fig. 2). In this lithofacies, Carignano et al. (2013) found an association of ostracods and charophytes.

*Interpretation*. The relatively fine grain size could indicate subaqueous processes of sedimentation arising from settling through a stationary water column. This interpretation is supported by the presence of the ostracod and charophyte fossils.

4.4. Reconstruction of the depositional palaeoenvironment

The paucity of preserved sedimentary structures makes the reconstruction of the depositional processes of Los Llanos Formation problematic. Extensive beds of pebbly sandstone that represent elements with erosive bases and that are characterised internally by wide and shallow troughs suggests deposition from unconfined flows, probably distributed by numerous, small and shallow channels directed to the WNW. Laminated sandstone beds with planar and laterally extensive contacts are also a common deposit from the upper regime flow in unconfined flows (Banham and Mountney, 2014). Tunbridge (1984) described Devonian parallel laminated sandstone formed by unconfined flows in distal and medial portion of fluvial distributive systems; similar lithofacies were reported by Nichols (2005), Nichols and Fisher (2007), Jordan and Mountney (2010) and Basilici et al. (2016) for sheet-like deposits in alluvial plain palaeoenvironments developed in semiarid climatic settings. Fielding (2006) demonstrated that alluvial-plain deposits with these structures can be produced in climate conditions characterised by a marked seasonality with precipitation concentrated over short durations in each year.

Medium- and fine-grained sandstone and pebbly sandstone have analogous compositional features, which are indicative of source provenance from felsic magmatic and clastic sedimentary rocks. Considering the poorly rounded conglomerate clasts and the paleodirection of the depositional flows, it is likely that the sediment source of the parent material was mainly derived from the reworking of

local lower Palaeozoic migmatitic and granitic complexes, which are exposed less than 2 km towards east (Fig. 1).

Quartz-grain microtextures of the coarse portion of the groundmass of the parent material of palaeosols can be a useful tool to understand previous transport mechanisms of sand grains (cf. Stoops et al., 2010). Two main transport processes for quartz grains were identified: aeolian and high-energy unidirectional subaqueous flows. Microtextures that indicate aeolian transport (low relief, upturned plates, rounded grain edges, silica adhering particles, bulbous edges and edge rounding) are very common, whereas microtextures associated with high-energy unidirectional subaqueous flows (v-shaped percussions cracks and conchoidal fractures) are less represented. Moreover, the microtextures suggest that the two mechanisms interacted in the transport and deposition of the sandstone. Figure 5F portrays aeolian generated microtextures (upturned plates), which overlap with subaqueous microtextures (conchoidal fractures with arcuate steps). This observation suggests that the sand was introduced into the area by high-energy, unconfined or poorly channelised subaqueous flows, and later reworked by wind action, as is common in semiarid environments (Almasrahy and Mountney, 2015; Cain and Mountney, 2009, 2011). Abundant pebble- to boulder-size clasts with ventifact morphology confirm long-lived wind action.

Muddy sandstone likely represents sediment accumulation via suspension settling in small lakes or ponds. Ostracod and charophyte fossils support a lake interpretation (Carignano et al., 2013).

The depositional areas were most likely represented by the distal part of a drainage system, possibly as a system of coalescent alluvial fans (*bajadas*) developed at the basin margin under the influence of a semiarid climate regime. Intermittent and largely unconfined subaqueous flows punctuated long episodes of aridity during which sand was reworked by aeolian processes (Fig. 6E). Small lakes were likely present in the distal parts of this system.

5. PALAEOSOLS AND PEDOGENIC PALAEOENVIRONMENT

The sedimentary succession of Los Llanos Formation exposed in Tama shows two pedotypes: Tama and Colozacán pedotypes.

5.1. Tama pedotype: description

This pedotype comprises 69% of the thickness of the measured succession (Fig. 2) and it is formed by palaeosol profiles characterised by A-Bw-Bk-C(k) horizons (Fig. 7). Most of the palaeosol profiles studied are characterised by alternations of Bw-Bk horizons (Fig. 8A). The thickness of the pedotype example is 0.4 to 2.5 m. Parent material is composed of poorly to moderately sorted, fine to medium-grained sandstone, with less than 5% granules and pebbles.

The A horizon is pale reddish orange (2.5YR7/3), no more than 0.15 m thick (Fig. 7 and 8B); this horizon is rarely preserved and it has been identified in only a two cases, based on high concentration of root traces (cf. Retallack, 1991).

The Bw horizon is 0.2 to 2.3 m thick, pale reddish orange (2.5YR7/3 or 7/4) in colour (Fig. 7 and 8A). This horizon displays root traces, mottles, abundant weatherable minerals, high thickness, absence of pedogenic structures and of macroscopic evidence of clay illuviation. Light grey (5Y8/1 or 10Y8/1) mottles, less than 20% in abundance, are present in some cases (Fig. 8C). Four types of root traces have been recognised: small, medium chalcedony, medium carbonate and large. Small root traces are the most abundant; they consist of thin (0.5-1 mm in diameter) and short (up to 10 mm long), contorted cylinders of white calcium carbonate, commonly bifurcated at acute angles and internally empty (Fig. 8D). Medium chalcedony type is formed of a vertical or subvertical cylinder, more than 0.2 m long, with circular section 3-15 mm in diameter, and with downward branching and tapering (Fig. 8E). The chalcedony fills the molds left by roots; sometimes, small vugs reveal an incomplete filling. Medium carbonate type is characterised by vertical cylinders of floating sandstone grains in microcrystalline calcite. Cylinders are 0.1-0.5 m long, with circular section 7-25 mm in diameter.

Large type root traces are represented by column-like forms, more than 4 m long, circular or elliptical in section (long axis 0.32-0.65 m). These column-like forms possess a calcium carbonate cemented sandstone ring, up to 40 mm thick, and an internal filling composed of material derived from overlying horizons (Fig. 8F).

The microfabric of Bw horizon is characterised by poorly sorted sandstone with brownish yellow (10YR6/6) micromass at plane polarised light (Fig. 9A). The related distribution pattern (coarse versus fine – c/f) is close or single-spaced gefuric to chitonic (Fig. 9A). Rarely, granostriated b-fabric is present, but in general not all grains display clay coatings and any clay coatings present do not typically completely surround the grains (Fig. 3B and 9B). The microstructure is apedal; pellicular grain structure is observed in some cases. Textural pedofeatures consist of clay coatings (<20 $\mu$m in thickness) that irregularly and patchily cover the sand grains (Fig. 3B and 9B). Crystalline pedofeatures are coatings composed of chalcedony (5-100 $\mu$m thick), that continuously cover the rims of a void (Fig. 9B).

The Bk horizon is 0.08-0.83 m thick and more than 300 m in lateral extension; this is pale reddish orange (2.5YR7/3 or 7/4) in colour, in some cases with light grey (5Y8/1 or 10Y8/1) mottles (Fig. 7). Calcium carbonate accumulation is typical of this horizon and highlighted by the cementation by micritic calcite and notable abundance of carbonate nodules. Calcareous nodules are isolated or, less commonly, coalescent with undifferentiated or concentric internal fabric. Overall, the nodules are subspherical, ellipsoidal or ameboid, 3-120 mm across, 1-30% in abundance, with very abrupt outer boundaries. Some of these nodules show septarian structures, constituted by chalcedony (Fig. 9C).

The microfabric of Bk horizon is composed of poorly sorted fine-grained sandstone with calcite micromass ranging in size 2-10 $\mu$m and light olive brown (2.5Y5/4) in colour. The crystallitic b-fabric is typical of this horizon (Fig. 9D). The related distribution pattern of c/f is single to double spaced

porphyric (Fig. 9E). The prevalent microstructure is apedal. Crystallitic b-fabric is characteristic of this horizon. Sometimes subhedral calcite crystals (hypidiotopic) are present as coatings around sand grains. Chalcedony pedofeatures are present.

The C(k) horizon has been rarely identified with the presence of relic primary (i.e. original) sedimentary structures (Fig. 7). This horizon is pale reddish orange (2.5YR7/3 or 7/4) and 0.2-0.4 m thick. Root traces are present, but are less common than in Bw horizons. The microfabric is composed of poorly sorted sandstone and the related distribution pattern (c/f) is monic.

In the Tama pedotype, silica is present (but not abundant), like fibrous cryptocrystalline (chalcedony), micro- and macrocrystalline (druse-like quartz crystals) forms. Crypto- and microcrystalline quartz fills the intergranular porosity or substitute calcite (Figs 9B and D). Druse-like quartz macrocrystals occur in larger vugs, where they occupy the central portion (Fig. 9F).

Fossil vertebrate skeletal remains of turtles, notosuchian crocodiliforms, sauropods, and theropods remains - isolated or articulated - are common in the Tama pedotype (Hechenleitner et al. 2014; Fiorelli et al., 2016). Fossil bones are in general well-preserved; typically, they do not display cracks or desquamated surfaces.

Molecular Weathering Ratios (MWR) were used to define weathering of the palaeosol profiles, clay and carbonate accumulation, and characteristics of the parent material. Table 3 shows the geochemical values of the examined samples; table 4 and figure 10 display the vertical distribution in palaeosol profiles of the Molecular Weathering Ratios (MWR) used in this study. The Ba/Sr molecular ratio may be used as weathering proxy (Sheldon and Tabor, 2009). Sr is more soluble than Ba, which is a relatively immobile element in environments subject to low or moderate rates of weathering. In the studied palaeosol profiles, values of Ba/Sr are low, varying from 0.42 to 2.35, and show the same trend in the same palaeosol profile. $\Sigma Bases/Al_2O_3$ gives information on the accumulation of insoluble products (such as clay, represented by alumina) in respect to soluble compounds ($Ca^{2+}$, $Mg^{2+}$, $Na^+$,

K^{+}) released by the hydrolytic alteration (hydrolysis). The palaeosol profiles of the Tama pedotype show hydrolysis values from 0.9 to 30. The values of $Al_2O_3/SiO_2$ (accumulation of clay or clayeyness) vary from 0.02 to 0.03, being virtually uniform in all the examined palaeosol profiles. Carbonate accumulation (calcification) is defined by the ratio of $(CaO+MgO)/Al_2O_3$, which varies from 0.3 to 25.6. The ratio of $TiO_2/Al_2O_3$ ratio was used to define the provenance and the homogeneity along the profile of the parent material. The results display homogeneous values from 0.04 to 0.05.

## 5.2. Tama pedotype: interpretation

The Tama pedotype displays evidence that can be attributed to weak pedogenic maturity. Macro- and microstructures (peds) are absent. Clay coatings cover sand grains in the Bw horizon, testifying to clay illuviation. However, as (i) the clay covering is patchy and irregular on grain surfaces, (ii) not all the grains display clay coatings and (iii) the coatings are not laminated or compound small amount of the clay was transported to B horizon. Clayeyness ($Al_2O_3/SiO_2$), which provides evidence relating to the mechanisms of clay formation and its illuviation, display extremely low (0.02 to 0.04) and uniform values in the Tama pedotype, suggesting poor formation and accumulation of clay in the soil profile. Thus, it was not possible to identify an argillic horizon (Bt). Carbonate accumulation in the Bk horizon is compared with the Stage II of Gile et al. (1966) and Machette (1985), which – although many factors influence the concentration of $CaCO_3$ into the soil – corresponds to development times between $10^4$ to $2x10^5$ years (Machette, 1985). Ba/Sr ratio increases with residence time and drainage conditions of the soil from 2 to 10 in weathered, well-drained and well-developed soils (Retallack, 1997). In the Tama pedotype, Ba/Sr values, which are equal or less than 2.35 and similar to those recorded in C horizons (interpreted to have geochemical signature close to the parent material), indicate low leaching of this pedotype (cf. Retallack and German-Heins, 1994). It should be noted that the lowest values of Ba/Sr are associated with high $CaCO_3$ content in the horizons, and are due

to substitution in carbonates of Ca by Sr (Buggle et al., 2011). $\Sigma$Bases/$Al_2O_3$ allows determination of the degree of weathering for hydrolysis. The values of $\Sigma$Bases/$Al_2O_3$ in Bw horizons are between 0.9 and 10.4, and are similar to the C horizons; higher values are due to CaO accumulation in Bk horizons. Given that weathered soils show, in general, $\Sigma$Bases/Al2O3 values less than 0.5 (Sheldon and Tabor, 2009) and considering that the Bw horizons have values equivalent with C horizons, the Tama pedotype indicates low conditions of weathering for hydrolysis. Petrographic analyses confirm these aspects, displaying fresh weatherable minerals (Fig. 3B).

The $TiO_2$/$Al_2O_3$ ratio (Sheldon and Tabor, 2009) and the petrographic analyses suggest that the parent material was derived from weathering of felsic magmatic and secondary clastic sedimentary rocks. Moreover, homogeneous values of $TiO_2$/$Al_2O_3$ along the palaeosol profiles demonstrate the invariability of the parent material (Sheldon, 2006).

Two main horizons have been recognised: Bw and Bk. The first is defined as a cambic horizon because – although displaying some pedogenic features (root traces, absence of sedimentary structures, clay coatings, hydrolysis effects, mottles) – it does not show characteristics typical of other well-defined subsurface horizons. The Bk horizon (pedogenic calcrete) is recognised based on macroscopic, micromorphological and chemical concentrations of carbonates. Revealing low maturity, but greater than in Entisols, common alternation of Bw and Bk horizons and the absence of aspects that associate it to other orders enable classification of the Tama pedotype as an Inceptisol (Foss et al. 1983; Soil Survey Staff, 1999; Buol et al., 2011). According to the classification of Mack et al. (1993), the Tama pedotype can alternatively be classified as Calcic Protosol.

Silica (microcrystalline quartz or chalcedony) is homogenously distributed throughout the studied sedimentary succession, occupying the porous spaces or substituting calcium carbonate. Silica is post pedogenic and probably formed in response to groundwater flow (cf. Nash and Ullyott, 2007).

5.3. Colozacán pedotype: description

This pedotype constitutes 22% of the thickness of the measured section. It occurs in the lower portion of the succession (Fig. 2). This pedotype is 1-2 m thick, with Bt, Bk and Ck horizons (Fig. 11). The parent material is slightly coarser than that of the Tama pedotype, but with similar petrographic composition. The Bt horizon is 0.25-0.8 m thick, pale reddish orange (2.5YR7/3), and shows small ameboid light gray mottles (2.5GY8/1) (Fig. 12A). Chalcedony root traces or rhizotubules are present (Fig. 12B). The calcium carbonate content is slight. Granostriated b-fabric is present and abundant: sand-sized grains are completely surrounded by clay coatings up to 50 μm thick. (Fig. 12C). The Bk horizon is 0.15-1.2 m thick, light grey (7.5YR8/1) or white (10YR9/1), and it is characterised by a high concentration of calcium carbonate, highlighted by coalescent nodules or by a structureless calcic horizon (Fig. 12D). Sand-sized clasts floating in the micritic mass reach 40-50% in abundance. The Ck horizon is 0.3-0.75 m thick, light grey (7.5YR8/1) or white (10YR9/1) and preserves relic primary sedimentary structures (Fig. 11). Calcium carbonate content is represented by microcrystalline calcite cement and nodules.

5.4. Colozacán pedotype: interpretation

Abundant clay coatings on sand-sized grains allow recognition of argillic horizon (Bt), whereas the absence of calcium carbonate indicates leaching of this component from the Bt to the underlying Bk horizon. The high calcium carbonate accumulation in the Bk horizon of this palaeosol is of pedogenic origin because: (i) it is associated with ordered sets of palaeosol horizons, (ii) it is characterised by sharp top and a clear to gradual lower boundary distinctness, (iii) it is associated with drained and oxidized environmental conditions, as testified by pale reddish orange (2.5YR7/3) colour and clay coatings, and (iv) it is less than 2 m thick (Pimentel et al., 1996). The Bk horizon is comparable with

Stage III, and perhaps IV, of calcium carbonate morphology of Gile et al. (1966) and Machette (1985); thus it represents a relatively well-developed palaeosol.

This pedotype can be attributed to the order of Aridisols and suborder Calcids for the following reasons: (i) it is characterised by a Bt and well-developed Bk horizons and (ii) it does not contain organic matter. Following the classification of Mack et al. (1993), this palaeosol is Calcisol.

5.5. Pedogenic palaeoenvironment and interaction with the depositional processes

The Tama pedotype is interpreted as an Inceptisol, a type of soil that presently develops at all latitudes and in various moisture conditions with the exception of aridic (Foss et al. 1983; Buol et al., 2011). Although this order of soil does not indicate specific environmental conditions, several aspects of the Tama pedotype yield information on its pedogenic palaeoenvironment. Clay coatings and carbonate accumulation testify that, in general, this pedotype formed above the water table in well-drained conditions (Retallack, 2001; Ashley et al., 2014). Local and temporary conditions of water stagnation probably after precipitation and/or fluctuation of the water table are, however, suggested by light-grey mottles that are, in some cases, observed in Bw horizons. Root traces indicate relatively abundant vegetation. Small root traces can be interpreted as rhizocretions formed by calcite precipitation around small living roots; the hole at the centre of the cylinder arises due to the later rot of the root (Retallack, 2001; Kraus and Hasiotis, 2006). They can represent the roots of small herbaceous and seasonal plants (Retallack, 2001). Medium dimension chalcedony root traces are interpreted as holes left after death and rot of roots, and then filled by precipitation from silica-enriched ground waters. Medium carbonate root traces – rhizotubules of Kraus and Hasiotis (2006) – are the product of precipitation of micritic cement within the parent material located around the rhizosphere, probably during the life of the root. Large root traces correspond to long tap roots that formed a cemented rind around the rhizosphere during the life of the plant. At the death of the plant

and consequent rot of the root the hole was filled by material derived from overlying horizons. These structures are similar to the palaeorhizosphere of Genise et al. (2011). Large- and medium-dimension root traces are evidence of perennial plants; in particular, large roots, more than 4 m depth (tap roots), indicate plants that took advantage of the deep water table during the drier season, suggesting well-drained conditions of the soil (Retallack, 2001; Hembree and Hasiotis, 2007). The association of small and medium/large roots may indicate the presence of two types of vegetation: herbaceous seasonal plants and perennial plants, which may be associated with a climate regime characterised by marked seasonal distribution of the precipitation (Retallack, 1983, 1991, 2001).

Overall, calcium carbonate accumulation in soils (Bk horizons) means environmental conditions with water deficit. Goudie (1983) affirmed that calcium carbonate accumulation currently develops preferentially in areas with mean annual precipitation between 400-600 mm. Proposed formulae with which to reconstruct MAP (mean annual precipitation) based on CIA-K or $\Sigma Bases/Al_2O_3$ (Sheldon et al., 2002) are not applicable, because the values of CIA-K and $\Sigma Bases/Al_2O_3$ of Bw horizons are very similar to the C horizons (Sheldon and Tabor, 2009). Likewise, formulae reliant on establishment of the depth of Bk horizons (Retallack, 2005) are not applicable, due to the progressive variation of thickness of the horizons during the coeval pedogenesis and accumulation of parent material (see discussion below).

Overall, the Tama pedotype formed in well-drained conditions, in a semiarid palaeoenvironment characterised by water deficit, but with sufficient precipitation to sustain some diversified vegetation.

Inceptisols are soils characterised by weak maturity because they form on young topographic surfaces or in environmental conditions that inhibit well-developed soil development (Foss et al., 1983; Buol et al. 2011). Two main features suggest that the poor maturity of the Tama pedotype is due to continuous input of parent material that kept pace with the pedogenesis: (i) this pedotype has

over-thickened profiles (mean 1.2 m; maximum 2.5 m) and Bw horizons (mean 0.7 m; maximum 2.3 m); (ii) the boundaries between the palaeosol profiles are gradual or diffuse; compound palaeosol profiles (Morrison, 1978), characterised by interbedded deposits with preserved sedimentary structures and/or abrupt boundaries between the palaeosol profiles, are essentially absent. The large thickness of profiles and horizons, and the gradual or diffuse boundaries between the palaeosol profiles can be ascribed to a relatively slow but steady rate of sedimentation due to aeolian and/or subaqueous depositional processes. Slow sediment input permitted the incorporation of material into the soil without interruption of the pedogenic processes (cf. Kraus and Alsan, 1993; Kraus, 1999; Ashley et al., 2014). Inceptisols are typical of areas subject to high sedimentation rate (Hartley et al., 2012).

Thus, the Tama pedotype can be interpreted as a cumulative palaeosol profile. Cumulative (or accretionary) palaeosol profiles form on topographic surfaces subjected to steady accretion via sedimentary on-going processes. Such a condition develops when the sedimentation rate is near-continuous but slow enough to not impede the pedogenesis of the deposited material (McDonald and Busacca, 1990; Marriott and Wright, 1993; Kraus, 1999). In fluvial floodplains developed in semiarid settings, Daniels (2003) calculated that the rate of sedimentation, below which the pedogenesis keeps pace with the sedimentation, is 5 mm/year. Kraus (1999) asserted that cumulative soils form in overbank areas with deposition rates up to 10 mm/year. This suggests that, for sedimentation rates less than 5-10 mm/year, depending on the environmental conditions, new sediment is incorporated into the soil and cumulative soil profiles form. A semiarid climate likely slows down or inhibits some pedogenic processes, thus favouring the poor development of the palaeosols and formation of Inceptisols (Foss et al., 1983). However, the short residence time of the particles in the zone of active soil formation was the main controlling factor of the pedogenesis (cf. Marriott and Wright, 1993).

The Colozacán pedotype displays greater illuviation of clay in the Bt horizon and greater concentration of calcium carbonate in the Bk horizon compared to the Tama pedotype. Clay illuviation and carbonate concentration indicate well-drained palaeoenvironmental conditions with a net water deficit, similar to the Tama pedotype. However, the greater clay and calcium carbonate content suggest greater development time of Colozacán pedotype. It is therefore likely that the sedimentation rate in the lower part of Los Llanos Formation was slower, permitting development of soils of greater maturity.

6. THE TITANOSAUR EGG CLUTCHES

The egg clutches were found at a level 60 m above the base of the studied Los Llanos Formation succession (Fig. 2), close to the present topographic surface. During the excavation for the recovery of the eggs, a stratigraphic section 1.2 m thick was measured, analysed and sampled. The succession containing the egg clutches comprises three palaeosol horizons: Bw-Bk-Bw (Fig. 13A). The upper Bw horizon is *c.* 0.90 m thick (but the top is eroded by the present topographic surface). It is formed of pale reddish orange (2.5YR7/3 or 7/4), poorly sorted, fine- to medium-grained sandstone, with some light-grey (5Y8/1 or 10Y8/1) mottles in the lower portion (Fig. 13A and B). Calcareous rhizocretions and rhizotubules, and chalcedony root casts similar to those already described are common. Micromorphological analyses display related distribution pattern (coarse versus fine - c/f) gefuric to chitonic, occasional granostriated b-fabric are observable (Fig. 13C) and peds are absent. The transition to the lower Bk horizon is gradual. This latter is c. 0.2 m thick, pale reddish orange (2.5YR7/3 or 7/4) and can be distinguished in the field by the presence of very coarse calcareous nodules, 5-90 mm in diameter. Micromorphological features show crystallitic b-fabric and absence of peds. This horizon overlays, via a gradual transition, a lower Bw horizon, whose characteristics are similar to the upper Bw. Molecular weathering ratios (leaching, hydrolysis,

clayeyness, calcification, provenance) of the entire interval display values and vertical trends similar to those described for the Tama pedotype (Fig. 10). Surface microtextures of the quartz sand grains have already been discussed above; they show similarity with the parent material of the Tama pedotype (Figs 4 and 5). Thus, all these aspects demonstrate that the egg-bearing strata belong to the Tama pedotype.

Five egg clutches, which collectively contained 21 complete eggs and several eggshell fragments, have been recovered from this Bw horizon between the levels 0.1-0.4 m (Fig. 13A). In plan view, the largest clutch shows elliptical-elongated shape with superposed eggs (Fig. 13D). Overall, the eggs were found in close association with each other, 20-80 mm apart. The eggs are filled with the same surrounding sandstone material, and have an oblate ellipsoid form: the short vertical axis is 119 mm high, the horizontal axes are each 210 mm long (Fig. 13D). Morphological features and taxonomic identity are described in detail by Hechenleitner et al. (2016). Based on their analyses, these authors concluded the following: (i) the eggs belong to Titanosauria; (ii) they are preserved *in situ*; (iii) the eggs were incubated with environmental source heat in burial conditions; and (iv) the occurrence of multiple clutches in the same Bw horizons means that this represented a colonial nesting area.

## 7. PRESERVATION OF EGG CLUTCHES

The eggs were found within a Bw horizon of a poorly developed palaeosol, classified an Inceptisol, whose parent material has been interpreted as deposited by non-confined subaqueous flows, deposits of which were reworked by aeolian processes, on the distal part of an alluvial-fan *bajada*, at the margin of a developing basin (Fig 6E). Egg-clutch geometrical arrangement is not compatible with subaqueous transport: the eggs are intact, were located in the same horizon in close proximity, which collectively demonstrates that they are preserved *in situ* (Hechenleitner et al., 2016).

An important question is whether the titanosaurs laid the eggs on the surface in an "open nest" or within the soil. According to palaeoecological aspects of the titanosaur eggs, it is improbable that the egg-laying site was on the soil surface (Hechenleitner et al., 2016). Indeed, the high porosity of the titanosaur eggshells and the necessity of the embryo to maintain internal moisture in order to develop in a semiarid environment support the hypothesis of burrow-nesting in dug-out holes (Seymour, 1979; Deeming, 2006; Grigorescu et al., 2010; Vila et al., 2010; Hechenleitner et al., 2016).

In general, the preservation potential of fossil eggs and clutches in palaeosols is very low. Most palaeosols form in correspondence to a stable topographic surface, which is exposed to biological, chemical and physical alterations, each of which decrease the likelihood of long-term preservation of eggs. Moreover, excavation by other sauropods seeking to lay eggs, or by other animals for any other biogenic activities, trampling, root growth, chemical and physical weathering of the soil would not usually allow the preservation of whole eggs in life position. Thus, an important question arises: what kind of conditions permitted the preservation of the titanosaur egg-clutches within the Tama pedotype?

The sedimentary interval, within which the egg clutches are contained, has been interpreted as a cumulative palaeosol profile, i.e. a type of soil characterised by a steady accumulation of the topographic surface with indicative values below 2 to 10 mm/year (Wright and Marriott, 1996; Kraus, 1999; Daniels, 2003). In these conditions, whatever is placed on or within a cumulative soil will be quickly isolated by pedogenic weathering. The term "quickly" is relative to residence time, i.e. time in which a given object (e.g. eggs) is subject to conditions of pedogenic weathering (Marriott and Wright, 1993). The residence time depends on both the sedimentation rate and the depth within the soil to which weathering operates, which is typically ~2 m (Wright and Marriott, 1996), but could be less in semiarid environments (Nettleton and Peterson, 1983). This means that, for a sedimentation rate of 2 mm/year and for soil profile weathering to a depth of 2 m, an object placed on the soil

surface is subject to pedogenic alteration for $10^3$ years. The residence time decreases when the object is placed (buried) within the soil and also when the soil develops in a semiarid environment. Thus, objects placed within cumulative soils in semiarid settings have high preservation potential. Thus, assuming that the eggs were laid at several centimetres from the top soil, the progressive growth of the topographic surface should have quickly isolated them from pedogenic modifications, which could otherwise have caused partial or complete destruction (Fig. 14). This reasoning is consistent with the occurrence of relatively well-preserved fossil bones, most of which do not show weathered surfaces and in some cases have been found articulated (Beherensmeyer, 1991; Fiorelli et al., 2016).

Are the accumulations of titanosaur eggs at Tama nests or clutches? In general, an accumulation of intact and closely associated dinosaur eggs is defined in literature as a fossil nest or clutch. Many authors used either or both of these terms to refer to an egg accumulation (e.g., Tandon et al., 1995; Cojan et al., 2003; Van Itterbeeck et al., 2004; Díaz-Molina et al., 2007; Grigorescu et al., 2010; Paik et al., 2012). However, other authors (Chiappe et al., 2004; Salgado et al., 2007; Vila et al., 2010) restricted the fossil nest definition to cases where there is clear evidence that an organism has laid eggs in a site suitable to ensure successful egg incubation and hatching. Chiappe et al. (2004) defined sedimentological criteria for the recognition of nests in the geological record. According to these authors a nest is the structure where (i) multiple intact eggs are preserved in close proximity to each other, (ii) a voluntary excavation that cuts previous sedimentary structures is observed, (iii) a ridge of dug material is preserved at the borders of the excavation, and (iv) the filling of the excavation is different from the dug material (Fig. 15A). May these criteria to be considered necessary conditions to recognise a fossil nest in egg-bearing palaeosol of Tama? Probably not. The egg-bearing succession of Tama does not show any sedimentological or palaeopedological characteristic that permits a nest to be distinguished from a clutch. In the Tama pedotype, a nest (i.e.,

a voluntary excavation in cumulative and immature sandy soil, filled after oviposition with the same excavated material) would have the same sedimentological features as a clutch (i.e., an accumulation of eggs on a non-voluntary excavation of the soil surface) (Fig. 15B). As such, only the first criterion of Chiappe et al. (2004) is followed (multiple intact eggs preserved in close proximity to each other). The boundaries of an excavation cannot be recognised, because cumulative and immature palaeosols do not exhibit well-defined and differentiated horizons or sedimentary structures, and any filling material would have the same composition and texture as the dug material. In conclusion, we think that the sedimentological criteria of Chiappe et al. (2004) to define a fossil nest are inapplicable to the Tama site, probably because they are too restrictive to be applied as general rules to recognise fossil nests in cumulative palaeosols. Moreover, Grellet-Tinner et al. (2012) and Hechenleitner et al. (2015, 2016) disagree with the criteria of Chiappe et al. (2004) from the palaeobiologic standpoint. These authors sustain that a titanosaur nest is "any recognizable structure or modification of environment that is voluntarily made by the parents to oviposit their eggs" (Hechenleitner et al., 2015) and, *de facto*, the criteria of Chiappe et al. (2004) do not match with this definition.

## 8. CONCLUSIONS

Los Llanos Formation, exposed close to the locality of Tama, is a >70 m-thick sedimentary succession composed almost entirely of palaeosols. Two pedotypes are recognised: Tama and Colozacán pedotypes. The Tama pedotype represents 69% of the measured part of the formation, contains titanosaur egg clutches preserved in a poorly developed palaeosol (Inceptisol). The Colozacán pedotype is 22% of the measured succession and represent a more mature palaeosol that took longer to develop, though in similar palaeoenvironmental conditions of Tama pedotype.

Preserved sedimentary structures, quartz grain surface microtexture analysis on parent material of the palaeosol, and presence of ventifacts have enabled an interpretation of the depositional environment as the distal part of coalescent alluvial fans (*bajadas*), where fluvial and aeolian processes interacted.

The Tama pedotype sustained diversified vegetation (as testified by varied and abundant root traces) in drained conditions and a semiarid climate (as suggested by reddish colour of the horizons, clay coatings and calcium carbonate concentration). Low maturity, gradual to diffuse boundaries of the horizons and exaggerated thickness of the Tama pedotype, reaching 2.5 m, suggest a cumulative aspect of this palaeosol: a soil characterised by accretion of the topographic surface during coeval pedogenesis due to slow, but continuous, sedimentary processes.

Due to relatively abundant vegetation and drained soils, titanosaurs chose this area as a nesting site. The high porosity of the eggshell suggests that titanosaurs probably laid their eggs in burrowsso as to maintain the embryo with sufficient humidity in an environment subject to a semiarid climate. Drained soils are not generally suitable sites for the preservation of fossil remains such as eggs. Indeed, chemical alterations and translocations, physical contraction and expansion, animal trampling and digging, and root growth mean that any preservation of eggs in palaeosols is outstanding. However, cumulative soils do create suitable conditions for egg preservation. In cumulative soils, the continuous accretion of the topographic surface decreases the residence time of eggs within the soil, thereby reducing the time over which they are subject to weathering conditions and so enhancing the potential for them to be incorporated into the geological record, where they become preserved.

A question still remains open: are the other sites, where egg-bearing strata are associated with pedogenic features, characterised by cumulative palaeosols?

REFERENCES

Almasrahy, M.A., Mountney, N.P., 2015. A classification scheme for fluvial–aeolian system interaction in desert-margin settings. Aeolian Research 17, 67-88.

Ashley, G.M., Beverly, E.J., Sikes, N.E., Driese, S.G., 2014. Paleosol diversity in the Olduvai Basin, Tanzania: effects of geomorphology, parent material, depositional environment, and groundwater on soil development. Quaternary International 322-323, 66-77.

Banham, S.G., Mountney, N.P., 2014. Climatic versus halokinetic control on sedimentation in a dryland fluvial succession: Triassic Moenkopi Formation, Utah, USA. Sedimentology 61, 570-608.

Basilici, G., Dal' Bo, P.F., de Oliveira, E.F., 2016. Distribution of palaeosols and deposits in the temporal evolution of a semiarid fluvial distributary system (Bauru Group, Upper Cretaceous, SE Brazil). Sedimentary Geology 341, 245–264.

Beherensmeyer, A. K., 1991. Terrestrial Vertebrate Accumulations. In: Allison, P., Briggs, D. E. G. (Eds.), Taphonomy: Releasing the Data Locked in the Fossil Record. Plenum, New York, pp. 291–335.

Bojar, A.V., Grigorescu, D., Ottner, F., Csiki, Z., 2005. Palaeoenvironmental interpretation of dinosaur- and mammal-bearing continental Maastrichtian deposits, Haḇeg basin, Romania. Geological Quarterly 49, 205–222.

Bridge, J.S., 2003. Rivers and Floodplains. Blackwell, Oxford, UK, pp. 491.

Buggle, B., Glaser, B., Hambach, U., Gerasimenko, N., Marković, S., 2011. An evaluation of geochemical weathering indices in loess-palaeosol studies. Quaternary International, 240, 12-21.

Buol, S. W., Southard, R. J., Graham, R. C., McDaniel, O. A., 2011. Soil genesis and classification. Sixth edition. Wiley-Blackwell, Oxford, pp. 543.

Cain, S.A., Mountney, N.P., 2009. Spatial and temporal evolution of a terminal fluvial fan system: the Permian Organ Rock Formation, South East Utah, USA. Sedimentology 56, 1774-1800.

Cain, S.A., Mountney, N.P., 2011. Downstream changes and associated fluvial-aeolian interactions in an ancient terminal fluvial fan system: the Permian Organ Rock Formation, SE Utah. In: Davidson, S, Leleu, S. and North, C. (eds), From River to Rock Record, SEPM Special Publication 97, pp. 165-187.

Carignano, A.P., Hechenleitner, E.M., Fiorelli, L.E., 2013. Hallazgo de ostrácodos (Crustacea) Cretácicos continentales en la Formación Los Llanos, localidad de Tama, La Rioja. Ameghiniana 50 (suppl.), R39.

Carpenter, K., Hirsch, K.F., Horner, J.R., 1994. Dinosaur Eggs and Babies. Cambridge University Press, pp. 372.

Cheel, R.J., Middleton, G.V., 1986. Horizontal laminae formed under upper flow regime plane bed conditions. Journal of Geology 94, 489-504

Chiappe, L.M., Schmitt, J.G., Jackson, F.D., Garrido, A., Dingus, L., Grellet-Tinner, G., 2004. Nest structure for sauropods: Sedimentary criteria for recognition of dinosaur-nesting traces. Palaios 19, 89–95.

Chiappe, L.M., Jackson, F., Coria, R.A., Dingus, L., 2005. Nesting titanosaurs from Auca Mahuevo and adjacent sites: understanding sauropod reproductive behavior and embryonic development. In: Curry Rogers, K.A., Wilson, J.A., (Eds.) The Sauropods: Evolution and Palaeobiology. University of California Press, Berkeley, pp. 285–302.

Cojan, I., Renard, M., Emmanuel, L., 2003. Palaeoenvironmental reconstruction of dinosaur nesting sites based on a geochemical approach to eggshells and associated palaeosols (Maastrichtian, Provence Basin, France). Palaeogeography, Palaeoclimatology, Palaeoecology 191, 111–138.

Costa, P.J.M., Andrade, C., Mahaney, W.C., Marques da Silva, F., Freire, P., Freitas, M.C., Janardo, C., Oliveira, M.A., Silva, T., Lopes, V., 2013. Aeolian microtextures in silica spheres induced in a wind tunnel experiment: Comparison with aeolian quartz. Geomorphology 180–181, 120–129

Daniels, J. M., 2003. Floodplain aggradation and pedogenesis in a semiarid environment. Geomorphology 56, 225–242.

Deeming, D.C., 2006. Ultrastructural and functional morphology of eggshells supports the idea that dinosaur eggs were incubated buried in a substrate. Palaeontology 49, 171–185.

Díaz-Molina, M., Kälin, O., Benito, M.I., Lopez-Martinez, N., Vicens, E., 2007. Depositional setting and early diagenesis of the dinosaur eggshell-bearing Aren Fm at Bastus, Late Campanian, south-central Pyrenees. Sedimentary Geology 199, 205–221.

Ezpeleta, M., Dávila, F.M., Astini, R.A., 2006. Estratigrafía y palaeoambientes de la Formación Los Llanos (La Rioja): una secuencia condensada miocena en el antepaís fragmentado andino central. Revista Asociación Geologica Argentina 61, 171-186.

Fielding, C.R., 2006. Upper flow regime sheets, lenses and scour fills: extending the range of architectural elements for fluvial sediment bodies. Sedimentary Geology 190, 227–240.

Fiorelli, L.E., Grellet-Tinner, G., Alasino, P.H., Argañaraz, E., 2012. The geology and palaeoecology of the newly discovered Cretaceous neosauropod hydrothermal nesting site in Sanagasta (Los Llanos Formation), La Rioja, northwest Argentina. Cretaceous Research 35, 94–117.

Fiorelli. L.E., Leardi, J.M., Hechenleitner, E.M., Pol, D., Basilici, G., Grellet-Tinner, G., 2016. A new Late Cretaceous crocodyliform from the western margin of Gondwana (La Rioja Province, Argentina). Cretaceous Research 60, 194-209

Fisher, N. D., Jordan, T. E., Brown, L., 2002. The structural and stratigraphic evolution of the La Rioja basin, Argentina. Journal of South American Earth Sciences 15, 141–156.

Foss, J.E., Moormann, F.R., Rieger, S., 1983. Inceptisols. In: Wilding, L.P., Smeck, N.E., Hall, G.F. (Eds.), Pedogenesis and Soil Taxonomy. II. The Soil Orders, Development in Soil Science, Elsevier Vol. 11B, pp. 355–381.

García, R.A., Salgado, L., Fernández, M.S., Cerda, I., Paulina Carabajal, A., Otero, A., Coria, R. , Fiorelli, L.E., 2015. Palaeobiology of titanosaurs: reproduction, development, histology, pneumaticity, locomotion and neuroanatomy from the South American fossil record. Ameghiniana 52, 29–68.

Genise, J.F., Bellosi, E.S., Verde, M., González, M.G., 2011. Large ferruginized palaeorhizospheres from a Palaeogene lateritic profile of Uruguay. Sedimentary Geology 240, 85–96.

Gile, L.H., Peterson, F.F., Grossman, R.B., 1966. Morphological and genetic sequences of carbonate accumulation in desert soils. Soil Science 101, 347–360.

Goudie, A.S., 1983. Calcrete. In: Goudies, A.S., Pye, K. (Eds.), Chemical sediments and geomorphology. Academic Press, London, New York, pp. 93-131.

Grellet-Tinner, G., Chiappe, L., Norell, M., Bottjer, D., 2006. Dinosaur eggs and nesting behaviours: a palaeobiological investigation. Palaeogeography, Palaeoclimatology, Palaeoecology 232, 294–321.

Grellet-Tinner, G., Fiorelli, L.E., Salvador, R.B., 2012. Water vapor conductance of the Lower Cretaceous dinosaurian eggs from Sanagasta, La Rioja, Argentina: Paleobiological and

paleoecological implications for South American faveoloolithid and megaloolithid eggs. Palaios 27, 35–47.

Grigorescu D., Garcia, G., Csiki, Z., Codrea, V., Bojar, A.V., 2010. Uppermost Cretaceous megaloolithid eggs from the Haţeg Basin, Romania, associated with hadrosaur hatchlings: Search for explanation. Palaeogeography, Palaeoclimatology, Palaeoecology 293, 360–374.

Hartley, A.J.,Weissmann, G.S., Bhattacharayya, P., Nichols, G.J., Scuderi, L.A., Davidson, S.K., Leleu, S., Chakraborty, T., Gosh, P., Mather, A.E., 2012. Soil development on modern distributive fluvial systems: preliminary observations with implications for interpretation of paleosols in the rock record. In: Driese, S.G., Nordt, L.C. (Eds.), New Frontiers in Paleopedology and Terrestrial Paleoclimatology. Paleosols and Soil Surface Analog Systems. SEPM, Special Publication Vol. 104, pp. 149–158.

Harms, J. C., Southard, J. B., Spearing, D. R., Walker, R. G., 1975. Depositional Environments as Interpreted from Primary Sedimentary Structures and Stratification Sequences. Short Course Notes Vol. 2, SEPM, Tulsa, OK, pp. 161.

Hechenleitner, E.M., Fiorelli, L.E., Larrovere, M.A., Grellet-Tinner, G., Carignano, A.P., 2014. Comment on "Dynamic topography in South America" by Federico M. Dávila & Carolina Lithgow-Bertelloni. Journal of South American Earth Sciences 50, 93-94.

Hechenleitner, E.M., Fiorelli. L.E., Grellet-Tinner, G., 2015. What do giant titanosaur dinosaurs and modern Australasian megapodes have in common? PeerJ 3, e1341.

Hechenleitner, E.M., Fiorelli. L.E., Grellet-Tinner, G., Leuzinger, L., Basilici, G., Taborda, J.A., de la Vega, S.R., Bustamante, C.A., 2016. A new Upper Cretaceous titanosaur nesting site from La Rioja (NW Argentina), with implications for titanosaur nesting strategies. Palaeontology 59, 1–14.

Hembree, D.I., Hasiotis, S.T., 2007. Paleosols and ichnofossils of the White River Formation of Colorado: insight into soil ecosystems of the North American midcontinent during the Eocene-Oligocene transition. Palaios 22, 123–142.

Hirsch, K.F., 2001. Pathological amniote eggshell—fossil and modern. In: Tanke, D.H., Carpenter, K. (Eds.) Mesozoic Vertebrate Life, Indiana Univ. Press, Bloomington, pp. 378–392.

Jordan, O.D., Mountney, N.P., 2010. Styles of interaction between aeolian, fluvial and shallow marine environments in the Pennsylvanian-Permian Lower Cutler Beds, southeast Utah, USA. Sedimentology 57, 1357-1385.

Kim, S.B., Kim, Y.G., Jo, H.R., Jeong, K.S., Chough, S.K., 2009. Depositional facies, architecture and environments of the Sihwa Formation (Lower Cretaceous), mid-west Korea with special reference to dinosaur eggs. Cretaceous Research 30, 100–126.

Kraus, M.J., 1999. Palaeosols in clastic sedimentary rocks: their geologic applications. Earth-Science Reviews 47, 41–70.

Kraus, J.M., Alsan, A., 1993. Eocene hydromorphic paleosols: significance for interpreting ancient floodplain processes. Journal of Sedimentary Petrology 63, 453-463

Kraus, M.J., Hasiotis, S.T., 2006. Significance of different modes of rhizolith preservation to interpreting. Palaeoenvironmental and palaeohydrologic settings: examples from Palaeogene palaeosols, Bighorn Basin, Wyoming, U.S.A. Journal of Sedimentary Research 76, 633–646.

Krinsley, D.H., Friend, P.F., Klimentidis, R., 1976. Eolian transport textures on the surfaces of sand grains of Early Triassic age. Geological Society of America Bulletin 87, 130-132.

Laity, J.E., 1994. Landforms of aeolian erosion. In: Abrahams A.D., Parson A.J., (Eds.) Geomorphology of Desert Environments, Chapman & Hall, London, pp. 506–535.

Liang, X., Wen, S., Yang, D., Zhou, S., Wu, S., 2009. Dinosaur eggs and dinosaur egg-bearing deposits (Upper Cretaceous) of Henan Province, China: occurrences, palaeoenvironments, taphonomy and preservation. Progress in Natural Science 19, 1587–1601.

Limarino, O., Poma, P., 2008. Hoja Geológica 3166-I - Chamical (1:250 000). Boletin n.257, Servicio Geológico Minero Argentino, Buenos Aires, pp. 35.

López-Martinez, N., Moratalla, J.J., Sanz, J.L., 2000. Dinosaurs nesting on tidal flats. Palaeogeography, Palaeoclimatology, Palaeoecology 160, 153–163.

Machette, N.M., 1985. Calcic soils of the southwestern United States. In:Weide, D.L. (Ed.), Soils and Quaternary Geology of the Southwestern United States. Geological Society of America Special Paper Vol. 203, pp. 10–21.

Mack, G.H., James, W.C., Monger, H.C., 1993. Classification of palaeosols. Geological Society of American Bulletin 105, 129–136.

Madhavaraju, J., García y Barragán, J.C., Hussain, S.M., Mohan, S.P., 2009. Microtextures on quartz grains in the beach sediments of Puerto Peñasco and Bahia Kino, Gulf of California, Sonora, Mexico. Revista Mexicana de Ciencias Geológicas 26, 367-379

Mahaney,W.C., 2002. Atlas of Sand Grain Surface Textures and Applications. Oxford University Press, Oxford, pp.237.

Margolis, S.V., Krinsley, D.H., 1971. Submicroscopic Frosting on Eolian and Subaqueous Quartz Sand Grains. Geological Society of America Bulletin 82, 3395-3406.

Margolis, S.V., Krinsley, D.H., 1974. Processes of formation and environmental occurrence of microfeatures on detrital quartz grains. American Journal of Science 274, 449-464.

Marriott, S.B., Wright, V.P., 1993. Palaeosols as indicators of geomorphic stability in two Old Red Sandstone alluvial suites, South Wales. Journal of the Geological Society of London 150, 1109–1120.

McDonald, E.V., Busacca, A.J., 1990. Interaction between aggrading geomorphic surfaces and the formation of a Late Pleistocene palaeosol in the Palouse loess of eastern Washington State. Geomorphology 3, 449-470.

Morrison, R.B., 1978. Quaternary soil stratigraphy—concepts, methods, and problems. In: Mahaney, W.C. (Ed.), Quaternary Soils. Geo-Abstracts, Norwich, pp. 77–108.

Nash, D.J., Ullyott, J.S., 2007. Silcrete. In: Nash, D.J. and McLaren S.J. (Eds.), Geochemical Sediments and Landscapes, Blackwell, Malden, Oxford, Victoria, pp. 95-143.

Nettleton, W.D., Peterson, P.F., 1983. Aridisols. In: Wilding, L.P., Smeck, N.E., Hall, G.F. (Eds.), Pedogenesis and soil taxonomy II. The soil orders. Developments in soil science 11B. Elsevier, Amsterdam, pp. 165–215.

Nichols, G.J., 2005. Sedimentary evolution of the Lower Clair Group, Devonian, West of Shetland: climate and sediment supply controls on fluvial, aeolian and lacustrine deposition. In: Doré, A.G., Vining, B.A. (Eds.), Petroleum Geology: North-West Europe and Global Perspectives—Proceedings of the 6th Petroleum Geology Conference, pp. 957–967.

Nichols, G.J., Fisher, J.A., 2007. Processes, facies and architecture of fluvial distributary system deposits. Sedimentary Geology 195, 75–90.

Paik, I.S., Huh, M., Kim, H.J., 2004. Dinosaur egg-bearing deposits (Upper Cretaceous) of Boseong, Korea: occurrence, palaeoenvironments, taphonomy, and preservation. Palaeogeography, Palaeoclimatology, Palaeoecology 205, 155–168.

Paik, S., Kim, H.J., Huh, M., 2012. Dinosaur egg deposits in the Cretaceous Gyeongsang Supergroup, Korea: Diversity and palaeobiological implications. Journal of Asian Earth Sciences 56, 135–146.

Pettijohn, F.J., Potter, P.E., Siever, R., 1987. Sand and Sandstone. Springer-Verlag, New York, pp. 553.

Pimentel, N.L., Wright, V.P., Azevedo, T.M., 1996. Distinguishing early groundwater alteration effects from pedogenesis in ancient alluvial basins: examples from the Palaeogene of southern Portugal. Sedimentary Geology 105, 1–10.

Retallack, G.J., 1983. A paleopedological approach to the interpretation of terrestrial sedimentary rocks: the mid-Tertiary fossil soils of Badlands National Park, South Dakota. Geological Society of American Bulletin 94, 823–840.

Retallack, G.J. (1991) Miocene Paleosols and Ape Habitats of Pakistan and Kenya. Oxford University Press, NewYork, pp. 346.

Retallack, G.J., 1994. The environmental factor approach to the interpretation of paleosols. In: Amundson, R., Harden, J., Singer, M. (Eds.), Factors in soils formation: a fiftieth anniversary retrospective. Soil Science Society of America Special Publication, Vol. 33, pp. 31–64.

Retallack, G.J., 1997. A colour guide to paleosols. Wiley, Chichester, pp. 175.

Retallack, G.J., 2001. Soils of the Past: an Introduction to Paleopedology. second ed. Blackwell, Oxford, pp. 404.

Retallack, G.J., 2005. Pedogenic carbonate proxies for amount and seasonality of precipitation in paleosols. Geology 33, 333–336.

Retallack, G.J., Germán-Heins, J., 1994. Evidence from Paleosols for the Geological Antiquity of Rain Forest. Science, Reprint Series 265, 499-502.

Salgado, L., Coria, R., Magalhaes Ribeiro, C.M., Garrido, A., Rogers, R., Simón, M.E., Arcucci, A.B., Curry Rogers, K., Carabajal, A.P., Apesteguía, S., Fernández, M., García, R., Talevi, M., 2007. Upper Cretaceous dinosaur nesting sites of Río Negro (Salitral Ojo de Agua and Salinas de Trapalcó-Salitral de Santa Rosa), Northern Patagonia, Argentina. Cretaceous Research 28, 392–404.

Salgado, L., Magalhães Ribeiro, C.M., García, R.A., Fernández, M.S., 2009. Late Cretaceous Megaloolithid eggs from Salitral de Santa Rosa (Río Negro, Patagonia, Argentina): inferences on the titanosaurian reproductive biology. Ameghiniana 46, 605–620.

Sander, P.M., Peitz, C., Gallemi, J., Cousin, R., 1998. Dinosaur nesting on a red beach? Comptes Rendues de la Académie des Sciences de Paris. Sciences de la Terre et des Planets 327, 67–74.

Saneyoshi, M., Watabe, M., Tsogtbaatar, K., 2008. Aeolian environments, palaeo-winddirection and dinosaur habitats of the Upper Cretaceous Djadokhta Formation, central Gobi Desert, Mongolia. Abstracts with Programs, Joint Meeting of Geological Society of America 40, 481.

Schoeneberger, P.J.,Wysocki, D.A., Benham, E.C., Soil Survey Staff, 2012. Field Book for Describing and Sampling Soils, Version 3.0. Natural Resources Conservation Service, National Soil Survey Center, Lincoln, NE, pp. 9-14.

Seymour, R.S., 1979. Dinosaur eggs: gas conductance through the shell, water loss during incubation and clutch size. Paleobiology 5, 1–11.

Sheldon, N.D., 2006. Abrupt chemical weathering increase across the Permian–Triassic boundary. Palaeogeography, Palaeoclimatology, Palaeoecology 231, 315– 321.

Sheldon, N.D. and Tabor, N.J., 2009. Quantitative paleoenvironmental and paleoclimatic reconstruction using paleosols. Earth Science Reviews 95, 1–52.

Sheldon, N.D., Retallack, G.J., Tanaka, S., 2002. Geochemical climofunctions from North America soils and application to paleosols across the Eocene–Oligocene boundary in Oregon. Journal of Geology 110, 687–696.

Soil Survey Staff, 1999. Soil taxonomy. A basic system of soil classification for making and interpreting soil surveys. US Department of Agriculture, Natural Resource Conservation Service, Washington, D.C., pp. 871.

Stoops, G., Marcelino, V., Mees, F., 2010. Micromorphological Features and Their Relation to Processes and Classification: General Guidelines and Keys. In: Stoops G., Marcelino, V., Mees, F. (Eds.), Interpretation of Micromorphological Features of Soils and Regoliths. Elsevier, Amsterdam, pp. 15-25.

Tandon, S.K., Good, A., Andrews, J.E., Dennis, P.F., 1995. Palaeoenvironments of the dinosaur-bearing Lameta Beds - Maastrichtian, Narmada Valley, Central India. Palaeogeography, Palaeoclimatology, Palaeoecology 117, 153–184.

Tunbridge, I.P., 1984. Facies model for a sandy ephemeral stream and clay playa complex; the Middle Devonian Trentishoe Formation of North Devon, U.K. Sedimentology 31, 697–715.

Van Itterbeeck, J., Sasaran, E., Codrea, V., Sasaran, L., Bultynck, P., 2004. Sedimentology of the Upper Cretaceous mammal- and dinosaur-bearing sites along the Râul Mare and Barbat rivers, Hateg Basin, Romania. Cretaceous Research 25, 517–530.

Van Itterbeeck, J., Horne, D.J., Bultynck, P., Vandenberghe, N., 2005. Stratigraphy and palaeoenvironment of the dinosaur-bearing Upper Cretaceous Iren Dabasu Formation, Inner Mongolian, People's Republic of China. Cretaceous Research 26, 699–725.

Vila, B., Jackson, F.D., Fortuny, J., Sellés, A.G., Galobart, A., 2010. 3-D modelling of megaloolithid clutches: insights about nest construction and dinosaur behaviour. PLoS ONE, 5, e10362.

Vujovich, G., Chernicoff, C.J., Tchilinguirian, P., Godeas, M., Marín, G., Pezzutti, N., Sepúlveda, E., 2007. Hoja Geológica 3166-111 Chepes (1:250000). Boletín n. 251, Servicio Geológico Minero Argentino, Buenos Aires, pp. 65.

Vos K., Vandenberghe N., Elsen J., 2014. Surface textural analysis of quartz grains by scanning electron microscopy (SEM): From sample preparation to environmental interpretation. Earth-Science Reviews 128, 93–104.

Wright, V.P., Marriott, S.B., 1996. A quantitative approach to soil occurrence in alluvial deposits and its application to the Old Red Sandstone of Britain. Journal of the Geological Society of London 153, 907-913.

CAPTIONS

Figure 1. Location of the study area and distribution of the main geological units. Granitoid complexes cropping out to the east of exposures of Los Llanos Formation are the possible source of the sandstone of this unit. Data simplified from geological map of Limarino and Poma (2008).

Figure 2. Simplified stratigraphic log of the measured section of Los Llanos Formation exposed near the town of Tama. The palaeosol profiles in the section are indicative; the single bed and the palaeosol horizon thickness are not to scale.

Figure 3.  (A) Poorly sorted, fine to medium-grained sandstone with subangular to rounded grains. PPL. (B) Photomicrography of feldspathic litharenite with monocrystalline quartz (a), lithic fragments (b) and feldspars (c). Thin and discontinuous clay coatings (d) cover some sand grains in Bw horizon. XPL. (C) Planar and undulated laminations are very uncommon in the studied sedimentary succession. They are interpreted as deposited by subaqueous flows in upper flow regime. Coin: 23 mm diameter.

Figure 4. Frequency distribution of quartz grains occurring with specific microtextures of the samples at 25 m and 60 m position of the stratigraphic section. The latter is the site of recovery of the egg clutches. See text for explanation.

Figure 5. Photomicrography of quartz grains. (A) Grain from egg clutches site. Rounded grain outline, with low relief, bulbous edges (a) and elongated depression (b). (B) Enlargement of yellow square of figure 5A, where upturned plates (a), v-shaped percussion cracks (b) and adhering particles (c) are visible. (C) Grain from 25 m level of the sedimentary succession (Fig. 2). Rounded grain outline, with low relief, edge rounding, bulbous edges (a) and conchoidal fracture (b) surface microtextures. (D) Enlargement of yellow square of figure 5C showing upturned plates (a), v-shaped percussion cracks (b), solution pits (c) and graded arc (d) surface microtextures. (E) Grain from the site of the egg clutches showing upturned plates (a), adhering particle (b) and probably v-shaped percussion cracks (c). (F) Grain from the 25 m level of the sedimentary succession (Fig. 2). Upturned plates (a) cover a conchoidal fracture (b) with arcuate steps (c). See the text for detail.

Figure 6. (A) Boulder ventifact found in pebbly sandstone. Hammer: 0.28 m. (B) Trough cross-stratified pebbly sandstone is located in Ck palaeosol horizon at the base of Los Llanos Formation. The Jacob's staff subdivisions are 0.1 m. (C) Circular histogram of palaeodirection data from trough cross-stratifications of pebbly sandstone. Palaeocurrents and petrographic data indicate provenance from local granitoid substratum. (D) The muddy very fine-grained sand intervals, containing ostracods, charophytes suggests subaqueous deposition in small lakes or ponds. (E) Reconstruction of the depositional system of Los Llanos Formation in Tama area. See text for explanation.

Figure 7. Tama pedotype profile. This pedotype is interpreted as a cumulative, poorly developed palaeosol (Inceptisol or calcic Protosol).

Figure 8. (A) Picture showing a vertical succession of Bw and Bk horizons. Cemented horizons are easily recognizable since they show appreciable relief on natural exposures. Note the gradual to diffuse transition between the horizons. The Jacob's staff subdivisions are 0.1 m. (B) The high concentration of root casts, chalcedony filled, likely identifies an A horizon. (C) Light-grey (5Y8/1 or 10Y8/1) mottles sometimes occur in Bw horizon. They suggest local and temporary water stagnation. Pencil: 142 mm. (D) Small cylindrical tubes of sparitic calcite (arrow), interpreted as rhizocretions, probably represent roots of small seasonal plants. Coin: 23 mm. (E) Medium chalcedony root traces (see arrow). The chalcedony filling occurred after pedogenesis due to precipitation of the silica in the hole left after the death of the root. Coin: 18.2 mm. (F) Large root traces, interpreted as tap roots of trees or large shrubs. They are largely diffused in Los Llanos Formation and can entry, as in the displayed case, within the weathered granitoid bedrock. Hammer (circled): 0.28 m length.

Figure 9. Tama pedotype. (A) Chitonic related distribution pattern of Bw horizon, PPL. (B) Bw horizon. Granostriated b-fabric (a) constituted of few clay coatings around the sand grains. Chalcedony constitutes coatings (b) and fills the packing voids (c). XPL. (C) Bk horizon. Isolated calcium carbonate nodules. In this case, the nodules display septarian structures, in which radial fractures are filled by chalcedony (see arrows). Pencil: 142 mm. (D) Bk horizon. Crystallitic b-fabric formed by different mosaics of calcite crystals with chalcedony (a) replacing the calcite, XPL. (E) Bk horizon. Rounded or subrounded clasts with porphyric related distribution, XPL. (F) Large vugs, up to 0.1 m, display chalcedony crystallization at the wall and druse-like macroquartz at the centre. Coin: 18.2 mm diameter.

Figure 10. Molecular Weathering Ratios (MWR) of Tama pedotype. Leaching: Ba/Sr; hydrolysis: $(CaO+MgO+Na_2O+K_2O)/Al_2O_3$; clayeyness: $Al_2O_3/SiO_2$; calcification: $(CaO+MgO)/Al_2O_3$; provenance:

$TiO_2/Al_2O_3$. The position in the general stratigraphic section of the three intervals of palaeosol profiles is indicated in figure 2.

Figure 11. Colozacán pedotype. This pedotype is interpreted as a well-developed palaeosol in semiarid and drained conditions (Aridisol or Calcisol).

Figure 12. Colozacán pedotype. (A) Pale reddish orange (2.5YR7/3) Bt horizon with light-grey (2.5GY8/1) mottles. The Jacob's staff subdivisions are 0.1 m. (B) Rhizotubules in Bt horizon. (C) Relatively abundant clay illuviation is indicated by granostriated b-fabric showing thick clay coating around the sand grains (see arrow), XPL. (D) Bk horizon constituted by structureless calcic horizon The Jacob's staff subdivisions are 0.1 m.

Figure 13. (A) Section of the cumulative poorly developed palaeosol (Tama pedotype) where the egg clutches were recovered. MWR from geochemical data of this palaeosol profile are shown in figure 10. (B) Various eggshell fragments (see arrows) in the pale reddish orange (2.5YR7/3 or 7/4), poorly sorted sandstone of the Bw horizon. Pencil: 142 mm. (C) Microphotograph of Bw horizon. Unweathered perthite (a) and quartz (b) grains are in places covered by clay coatings (see arrows). (D) Eggs of titanosaurs in one of the recovered clutches. The eggs lie close to each other suggesting that they are in their original position. The egg on the left is barely exposed because it is located at a lower position relative to the other egg on the right.

Figure 14. Model of laying and preservation of titanosaur egg clutches in Tama pedotype. See text for explanation.

Figure 15. (A) Model of events that lead to the preservation of titanosaur nests according to Chiappe et al. (2004), modified from the same authors. I: Excavation and laying of the eggs; II: flood; III: deposition and burying of the eggs. (B) Model of events that lead to the preservation of a titanosaur nests in the Tama pedotype. I: Selection of the laying area; II: excavation, laying and covering of the eggs; III: new deposition. Note that, in this model, most of the features that Chiappe et al. (2004) indicated as prerogative of the identification of a nest are not evident.

Table 1.

Summary of the features and interpretation of deposits of Los Llanos Formation.

Table 2.

Summary of the features and interpretation of palaeosols of Los Llanos Formation.

Table 3.

Weight percentage of the major oxides and ppm of trace elements within the Tama pedotype profiles of figure 10.

Table 4.

Values of the Molecular Weathering Ratios used in this study. These values are shown in graphic of figure 10.

Table 1

| Deposits | Description | Interpretation | Figures |
|---|---|---|---|
| Sandstone | <u>Textural features</u>. Subangular to well-rounded, poorly to moderately sorted, medium- and fine-grained sand grains with sparse granules and small pebbles; clastic fraction finer than coarse silt is less than 20%.<br><u>Petrographic composition of the sand grains</u>. Monocrystalline quartz (46.1-76.8% in abundance), feldspars (4.7-20.4) and lithic fragments (11.1-37.8%).<br><u>Sedimentary structures and bed geometry</u>. Very rare planar, undulating and parallel laminations, no more than 0.2 m thick and more than 5 m laterally extended. Such beds always occur directly above the top of palaeosol profiles. The laminations are revealed by alternations of fine-grained sandstone (1 to 4 mm thick) and medium-grained sandstone (<1 mm thick), with no evidence of grain-size grading. | Sheet flow deposits formed by subaqueous processes reworked by aeolian processes. These deposits probably formed on the distal portion of coalescent alluvial fans. | Figs. 3, 6E |
| Pebbly sandstone (conglomerate) | <u>Textural features</u>. Poorly sorted, medium to coarse-grained sand with granule to boulder clasts. Pebble and larger clasts are very angular to subrounded. Ventifacts occur.<br><u>Composition of the granule to boulder clasts</u>. Vein quartz (82% in abundance), feldspars (7%) and very fine-grained sandstone (5%); clasts of rhyolite, quartzite and granite comprise the remaining 6%. The sandstone component has analogous petrographic characteristics sandstone lithofacies described above.<br><u>Sedimentary structures and bed geometry</u>. This lithofacies is formed of tabular beds, 1 to 2.1 m thick and more than 2 km laterally extended. The bottom surfaces are erosive and characterised by scours up to 2 m wide and 0.5 m deep. Poorly preserved primary sedimentary structures take the form of trough cross-stratified sets, each 0.3-0.5 m thick. | Deposition by non- or poorly channelised subaqueous flows, probably characterised by a high and ephemeral hydraulic regime, coming from ESE. The deposition probably occurred on the intermediate or distal portion of coalescent alluvial fans. | Figs. 6A, 6B, 6C and 6E |
| Muddy sandstone | <u>Textural features</u>. Unconsolidated, dull orange (2.5YR6/3), muddy sand. The sand is very fine in grain-size, moderately sorted and structureless.<br><u>Bed geometry</u>. This lithofacies forms two lenticular beds, each up to 4 m thick and up to 200 m in lateral extent. These beds possess sharp lower and upper boundaries. | Deposition in calm water of temporary small lake or ponds, probably formed on the distal portion of coalescent alluvial fans. | Figs. 2 and 6D, 6E |

Table 2

| Palaeosols | Description | Interpretation | Figures |
|---|---|---|---|
| Tama pedotype | Parent material: poorly to moderately sorted, fine to medium-grained sandstone, with less than 5% granules and pebbles<br>A horizon: pale reddish orange (2.5YR7/3), less than 0.15 m thick. Abundant root traces.<br>Bw horizon: pale reddish orange (2.5YR7/3 or 7/4), 0.2 to 2.3 m thick. The distinctness of this horizon boundary is gradual to diffuse; the topography smooth to wavy. Roots, light grey (5Y8/1 or 10Y8/1) mottles, with boundary distinctness clear or gradational. Abundant weatherable minerals, high thickness. Absence of pedogenic structures. In a few cases, the Bw horizon is light grey in colour and shows pale reddish orange (2.5YR7/3 or 7/4) mottles that themselves represent 30-40% of the horizon. Close or single-spaced gefuric to chitonic related distribution pattern; rare granostriated b-fabric; apedal microstructure. Complex packing voids (20-150 ꭑm) (3-10% of the objective field) are partially or completely filled with chalcedony.<br>Bk horizon: pale reddish orange (2.5YR7/3 or 7/4) 0.08-0.83 m thick. The distinctness of this horizon boundary with Bw or C horizons is gradual or diffuse, and the topography is smooth, locally wavy. Calcium carbonate accumulation is represented by micritic cement and nodules, with undifferentiated or concentric internal fabric. Nodules with undifferentiated internal fabric are subspherical, ellipsoidal or ameboid, 3-120 mm across, 1-30% in abundance, on average 7%, with very abrupt outer boundaries. Internally these nodules are composed of microcrystalline calcite with sparse floating siliciclastic sandy grains, less than 15% in abundance. Nodules with concentric internal fabric are less abundant; they have subspherical or ellipsoidal form, locally are coalescent, 10-60 mm across, and in section they are composed of concentric rings, 1-5 mm thick, of microcrystalline calcite with floating siliciclastic sand grains, and of sparry calcite, less than 2 mm thick. Single to double spaced porphyric related distribution pattern. Crystallitic b-fabric. Apedal microstructure. Typic crystalline calcitic pedofeature. Rarely, and at the transition with the horizon Bw, striated b-fabric (in particular, discontinuous granostriated) is present. The size of the calcite varies from micrite to microsparite, with equigranular and xenotopic crystals. Subhedral calcite crystals (hypidiotopic) are locally present as coatings around sand grains. Chalcedony pedofeatures comprise 3 to 25% of the objective field. They have irregular margins and appear to replace calcite crystals.<br>C(k) horizon: pale reddish orange (2.5YR7/3 or 7/4) and 0.2-0.4 m thick. The distinctness of the upper horizon boundary with Bw or Bk horizons is gradual to diffuse, whereas distinctness of the lower boundary with the Bw horizon is sharp or very sharp. The topography of the horizon boundaries is smooth or wavy. Primary sedimentary structures occur: planar or undulating laminations or cross stratifications. Monic related distribution pattern. | Cumulative poor developed Inceptisol formed in semiarid and drained paleoenvironmental conditions. | Figs. 2, 7, 8 and 9 |
| Colozacán pedotype) | Parent material: poorly<br>Bt horizon: pale reddish orange (2.5YR7/3), 0.25-1.8 m thick. The distinctness and topography of the lower boundary with Bk horizon are sharp and smooth, respectively, whereas the distinctness and topography of the upper boundary with Bk horizon are clear to gradual and smooth to wavy, respectively. Upper boundary is with Ck horizon is sharp and wavy. Calcium carbonate content absent or low (<5% in abundance). No pedogenic structures. Light gray mottles (2.5GY8/1), up to 20% in abundance. Rhizotubules and chalcedony root traces are present. Abundant granostriated b-fabric; apedal microstructure.<br>Bk horizon: light gray (7.5YR8/1) or white, 0.15-1.2 m thick. Lower boundary with Ck horizon is diffuse and smooth. High calcium carbonate content: 50% in abundance or more. Crystallitic b-fabric is typical.<br>Ck horizon: light gray (7.5YR8/1) or white, 0.3-0.75 m thick. Calcium carbonate micritic cement and nodules occur. Relics of trough cross-beddings are present. Monic related distribution pattern. | Well-developed palaeosol formed in semiarid and drained paleoenvironmental conditions. Aridisol. | Figs. 2, 11 and 12 |

Table 3

## Major oxides (weight percentage)

| Sample | Horizon | Depth m | SiO$_2$ | TiO$_2$ | Al$_2$O$_3$ | Fe$_2$O$_3$ | MnO | MgO | CaO | Na$_2$O | K$_2$O | P$_2$O$_5$ | LOI | Total |
|---|---|---|---|---|---|---|---|---|---|---|---|---|---|---|
| LL6 | Bw | 0.1 | 89.19 | 0.192 | 4.83 | 1.01 | 0.017 | 0.48 | 0.59 | 0.75 | 1.31 | 0.03 | 1.41 | 99.8 |
| LL7 | Bw | 0.8 | 89.06 | 0.182 | 5.13 | 1.01 | 0.019 | 0.49 | 0.63 | 0.89 | 1.43 | 0.03 | 1.28 | 100.2 |
| LL8 | Bk | 1.05 | 42.08 | 0.085 | 2.29 | 0.5 | 0.019 | 0.38 | 29.35 | 0.43 | 0.55 | 0.03 | 24.2 | 99.9 |
| LL9 | Bw | 1.5 | 61 | 0.124 | 3.27 | 0.7 | 0.016 | 0.42 | 17.78 | 0.51 | 0.91 | 0.03 | 15 | 99.7 |
| LL10 | Bw | 1.95 | 71.5 | 0.135 | 3.9 | 0.94 | 0.017 | 0.46 | 11.39 | 0.58 | 1.08 | 0.03 | 9.72 | 99.8 |
| LL11 | Bw | 2.35 | 63.57 | 0.119 | 3.5 | 0.86 | 0.025 | 0.44 | 16.17 | 0.48 | 0.97 | 0.03 | 13.7 | 99.9 |
| LL12 | Bk | 2.8 | 37.64 | 0.074 | 2.02 | 0.51 | 0.037 | 0.36 | 32.14 | 0.31 | 0.49 | 0.03 | 26.3 | 99.9 |
| LL13 | Bwg | 3.55 | 81.5 | 0.113 | 3.31 | 0.64 | 0.019 | 0.33 | 6.6 | 0.55 | 0.95 | 0.03 | 5.84 | 99.9 |
| | | | | | | | | | | | | | | |
| LL14 | Bw | 0.85 | 90.1 | 0.159 | 4.31 | 0.94 | 0.018 | 0.42 | 0.55 | 0.66 | 1.2 | 0.03 | 1.36 | 99.8 |
| LL15 | C | 1.9 | 90.12 | 0.178 | 4.38 | 0.94 | 0.02 | 0.41 | 0.55 | 0.67 | 1.19 | 0.04 | 1.27 | 99.8 |
| LL16 | Bkg | 2.9 | 41.66 | 0.081 | 2.14 | 0.48 | 0.037 | 0.39 | 29.64 | 0.41 | 0.53 | 0.03 | 24.5 | 99.9 |
| LL17 | Bw | 3.1 | 90.48 | 0.151 | 4.08 | 0.78 | 0.018 | 0.38 | 0.33 | 1 | 1.13 | 0.03 | 1.23 | 99.6 |
| LL18 | Bw | 3.3 | 90.02 | 0.165 | 4.53 | 0.8 | 0.016 | 0.4 | 0.5 | 0.7 | 1.25 | 0.03 | 1.18 | 99.6 |
| LL19 | Bk | 3.6 | 42.12 | 0.086 | 2.21 | 0.46 | 0.033 | 0.34 | 29.49 | 0.4 | 0.57 | 0.03 | 24.2 | 99.9 |
| LL20 | Bw | 3.75 | 89.7 | 0.163 | 4.46 | 0.93 | 0.019 | 0.41 | 0.59 | 0.69 | 1.28 | 0.03 | 1.18 | 99.5 |
| LL22 | Bk | 4.3 | 61.67 | 0.113 | 3.31 | 0.7 | 0.021 | 0.36 | 17.51 | 0.55 | 0.95 | 0.037 | 14.1 | 99.3 |
| LL23 | Ck | 4.85 | 48.41 | 0.081 | 2.58 | 0.57 | 0.027 | 0.36 | 24.53 | 0.54 | 0.66 | 0.037 | 20.8 | 98.6 |
| | | | | | | | | | | | | | | |
| LLE1 | Bw | 0.2 | 89.14 | 0.19 | 4.77 | 1.01 | 0.016 | 0.44 | 0.51 | 0.76 | 1.21 | 0.03 | 1.37 | 99.4 |
| LLE2 | Bw | 0.6 | 90.02 | 0.178 | 4.38 | 0.91 | 0.02 | 0.41 | 0.48 | 0.7 | 1.17 | 0.04 | 1.24 | 99.5 |
| LLE3 | Bk | 1.05 | 62.49 | 0.091 | 2.76 | 0.58 | 0.021 | 0.32 | 17.54 | 0.48 | 0.79 | 0.059 | 14.1 | 99.2 |
| LLE4 | Bw | 1.2 | 76.96 | 0.109 | 3.18 | 0.61 | 0.012 | 0.31 | 9.13 | 0.54 | 0.91 | 0.041 | 7.83 | 99.6 |

## Trace elements (ppm)

| Sample | Horizon | Depth m | Ba | Ce | Cr | Cu | Ga | La | Nb | Nd | Ni | Pb | Rb | Sc | Sr | Th | V | Y | Zn | Zr |
|---|---|---|---|---|---|---|---|---|---|---|---|---|---|---|---|---|---|---|---|---|
| LL6 | Bw | 0.1 | 166 | <13 | 27.2 | 6.1 | 4.5 | <13 | 4.3 | <10 | 2.9 | 8.9 | 44 | <3 | 51 | 5.6 | 41 | 10.8 | 15.7 | 128 |
| LL7 | Bw | 0.8 | 175 | 15 | 15.6 | 6 | 5.1 | <13 | 4.5 | <10 | <2 | 11.5 | 48 | 4 | 58 | 4.4 | 47 | 11.8 | 17.4 | 137 |
| LL8 | Bk | 1.05 | 380 | <13 | 8.9 | <1.5 | 4.3 | 13.7 | 2.6 | 12 | 2.3 | 10.4 | 6.7 | 4 | 186 | 2.2 | 16.5 | 11.5 | 8.6 | 59 |
| LL9 | Bw | 1.5 | 166 | <13 | 4.3 | 2 | 4.7 | 15.1 | 3.1 | <10 | 3.2 | 8.2 | 20 | 4 | 142 | 3.3 | 25.9 | 12.5 | 11.5 | 83 |
| LL10 | Bw | 1.95 | 161 | <13 | 51 | 2.4 | 4.2 | <13 | 3.9 | 11 | 2.3 | 8.7 | 27 | 4 | 84 | 3.3 | 34 | 10.8 | 14 | 85 |
| LL11 | Bw | 2.35 | 152 | <13 | 5.7 | 2.2 | 4.1 | <13 | 3.4 | 14 | 3.8 | 9 | 21.8 | 4 | 111 | 4.5 | 26.6 | 11.2 | 13.5 | 81 |
| LL12 | Bk | 2.8 | 133 | <13 | 11 | <1.5 | 4.6 | <13 | 2.5 | <10 | 3.9 | 10.2 | 5.1 | 4 | 198 | 4.3 | 17.6 | 10.7 | 9.3 | 48 |
| LL13 | Bwg | 3.55 | 198 | <13 | 5.3 | 2.8 | 3.7 | <13 | 3.1 | <10 | <2 | 6.9 | 28 | 4 | 55 | 3.1 | 36 | 9.5 | 9.9 | 94 |
| | | | | | | | | | | | | | | | | | | | | |
| LL14 | Bw | 0.85 | 151 | <13 | 19.1 | 6.4 | 4.7 | <13 | 3.9 | <10 | 2.2 | 9.1 | 42 | 3 | 45 | 4.3 | 37 | 11.3 | 14.1 | 129 |
| LL15 | C | 1.9 | 150 | <13 | 10.1 | 6.4 | 4.2 | <13 | 4.1 | <10 | 2.4 | 9.1 | 43 | <3 | 45 | 5 | 36 | 12.5 | 13.1 | 124 |
| LL16 | Bkg | 2.9 | 131 | <13 | 17 | <1.5 | 4 | 19.6 | 2.7 | <10 | 3 | 10.9 | 6.2 | 5 | 139 | 2.4 | 16.1 | 12.7 | 9.4 | 61 |
| LL17 | Bw | 3.1 | 135 | <13 | 8.6 | 5.9 | 4.2 | <13 | 3.8 | 11 | 3.2 | 9.5 | 41 | <3 | 39 | 5.9 | 42 | 10.4 | 12.8 | 125 |
| LL18 | Bw | 3.3 | 151 | 15 | 25 | 6.5 | 4.7 | <13 | 4.1 | <10 | 3 | 11 | 45 | <3 | 45 | 5.3 | 37 | 11.7 | 13.2 | 137 |
| LL19 | Bk | 3.6 | 129 | <13 | 13.4 | <1.5 | 4.9 | <13 | 2.9 | 31 | 2.8 | 10.5 | 6.9 | 4 | 124 | 2.7 | 16.5 | 13.8 | 8.8 | 57 |
| LL20 | Bw | 3.75 | 170 | 15 | 18 | 5.6 | 4.3 | <13 | 4.1 | 12 | <2 | 11.5 | 44 | <3 | 46 | 5.6 | 37 | 11.5 | 14.1 | 131 |
| LL22 | Bk | 4.3 | 228 | 20 | 6.2 | <1 | 4.3 | <13 | 3 | 14 | 2.2 | 14.6 | 27.7 | 5 | 80 | 3.9 | 22 | 11.2 | 11.4 | 92 |
| LL23 | Ck | 4.85 | 407 | <13 | 9.7 | <1 | 3.3 | 14 | 3.3 | 26 | 3.1 | 14 | 19.5 | 6 | 97 | 3.8 | 16.4 | 10.7 | 10.7 | 70 |
| | | | | | | | | | | | | | | | | | | | | |
| LLE1 | Bw | 0.2 | 164 | <13 | 24.5 | 6.1 | 4.2 | <13 | 4.1 | <10 | 2.4 | 8.9 | 42 | <3 | 50 | 5.6 | 39 | 10.9 | 15.2 | 124 |
| LLE2 | Bw | 0.6 | 149 | <13 | 12.1 | 6.2 | 4.2 | <13 | 3.9 | <10 | 2.6 | 9.6 | 44 | <3 | 45 | 5.1 | 36 | 12.2 | 13.2 | 120 |
| LLE3 | Bk | 1.05 | 157 | <13 | 4.2 | <1 | 4.6 | <13 | 2.7 | <11 | 2.4 | 11.2 | 22 | 7 | 85 | 4.8 | 17.5 | 10.8 | 9.7 | 74 |
| LLE4 | Bw | 1.2 | 177 | <13 | 8.6 | 1.2 | 4.1 | <13 | 2.9 | 19 | <2 | 11.7 | 28.5 | 4 | 66 | 4.5 | 25.5 | 9.1 | 11.2 | 82 |

Table 4

| Sample | Horizon | Depth m | Leaching Ba/Sr | Hydrolysis | Clayeyness | Calcification | Provenience $TiO_2/Al_2O_3$ |
|---|---|---|---|---|---|---|---|
| LL6 | Bw | 0.1 | 2,076689 | 1,022401 | 0,031916 | 0,473395143 | 0,050748 |
| LL7 | Bw | 0.8 | 1,925057 | 1,05193 | 0,033947 | 0,464816943 | 0,045291 |
| LL8 | Bk | 1.05 | 1,30348 | 24,29054 | 0,032072 | 23,72168811 | 0,047386 |
| LL9 | Bw | 1.5 | 0,745853 | 10,76824 | 0,031593 | 10,21045968 | 0,04841 |
| LL10 | Bw | 1.95 | 1,22287 | 6,152483 | 0,032146 | 5,608099098 | 0,044191 |
| LL11 | Bw | 2.35 | 0,873684 | 9,243183 | 0,032448 | 8,717602922 | 0,043405 |
| LL12 | Bk | 2.8 | 0,428568 | 29,89355 | 0,031628 | 29,37853304 | 0,046767 |
| LL13 | Bwg | 3.55 | 2,296868 | 4,46136 | 0,023936 | 3,877361356 | 0,043583 |
|  |  |  |  |  |  |  |  |
| LL14 | Bw | 0.85 | 2,140908 | 1,031701 | 0,028192 | 0,478433334 | 0,047096 |
| LL15 | C | 1.9 | 2,12673 | 1,010724 | 0,028643 | 0,465013692 | 0,051881 |
| LL16 | Bkg | 2.9 | 0,601298 | 26,22586 | 0,030274 | 25,64262028 | 0,048321 |
| LL17 | Bw | 3.1 | 2,208527 | 1,08555 | 0,026575 | 0,38257626 | 0,047248 |
| LL18 | Bw | 3.3 | 2,140908 | 0,976837 | 0,029657 | 0,423966098 | 0,046499 |
| LL19 | Bk | 3.6 | 0,663746 | 25,22671 | 0,030923 | 24,649797 | 0,049679 |
| LL20 | Bw | 3.75 | 2,357896 | 1,038119 | 0,029303 | 0,472978621 | 0,046657 |
| LL22 | Bk | 4.3 | 1,818354 | 10,47692 | 0,031632 | 9,892926099 | 0,043583 |
| LL23 | Ck | 4.85 | 2,677049 | 18,26026 | 0,031409 | 17,63905681 | 0,04008 |
|  |  |  |  |  |  |  |  |
| LLE1 | Bw | 0.2 | 2,092702 | 0,96432101 | 0,031537 | 0,427652 | 0,05085079 |
| LLE2 | Bw | 0.6 | 2,112552 | 0,9879924 | 0,028675 | 0,435957 | 0,051881 |
| LLE3 | Bk | 1.05 | 1,178459 | 12,443362 | 0,02603 | 11,84746 | 0,04209154 |
| LLE4 | Bw | 1.2 | 1,711051 | 6,05553956 | 0,024352 | 5,466455 | 0,04375844 |
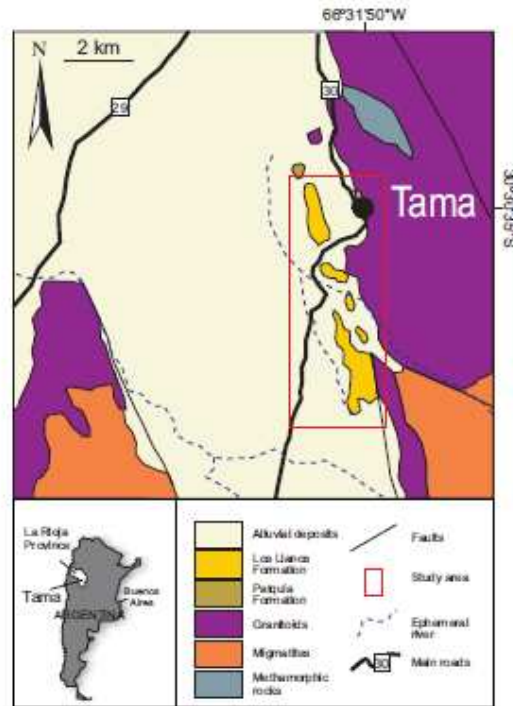
FIGURE 1
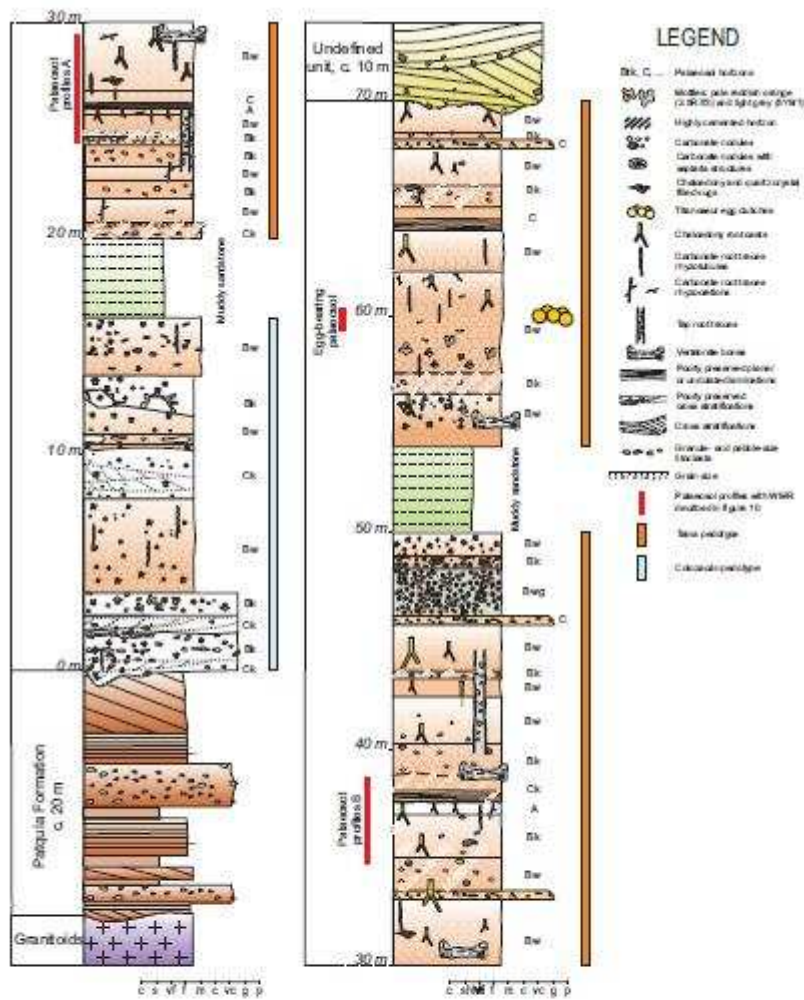
FIGURE 2
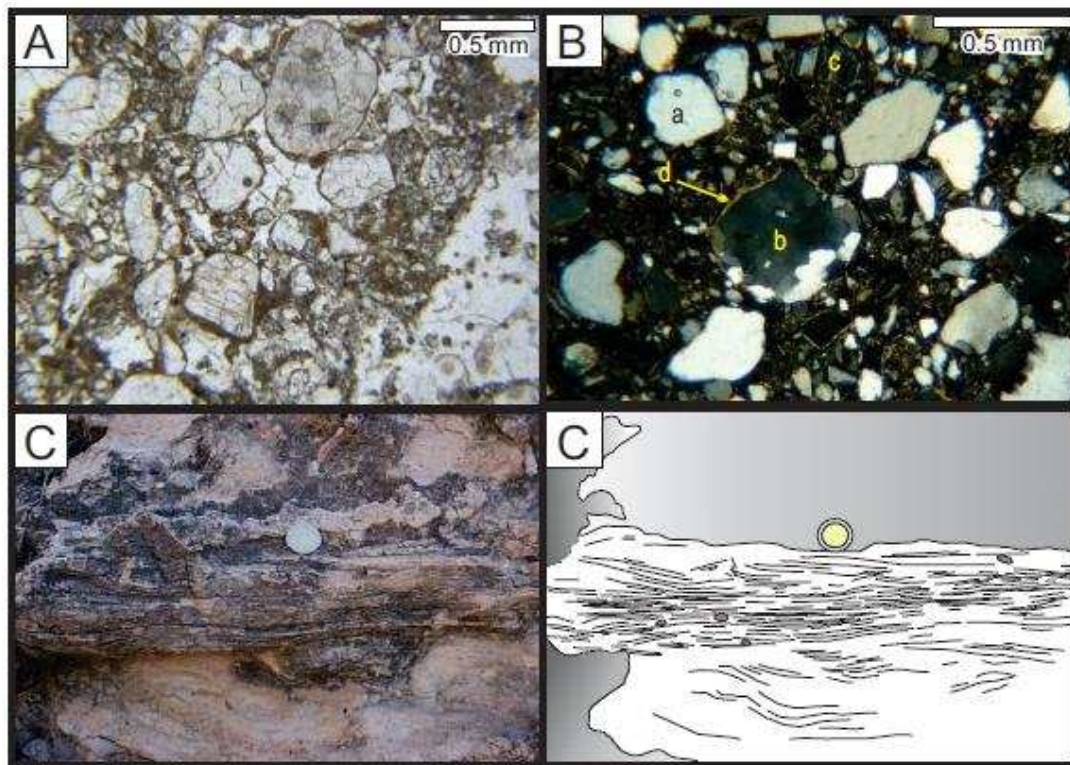
FIGURE 3
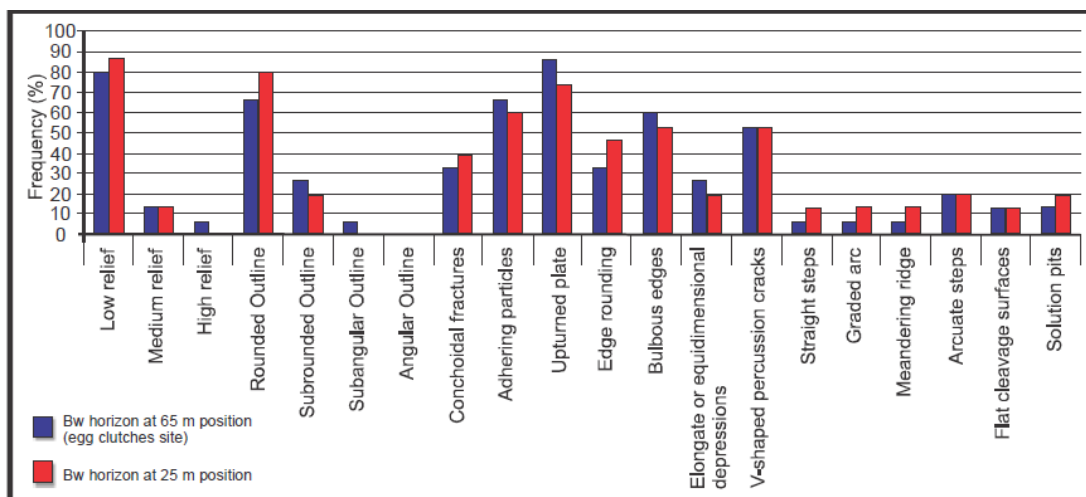
FIGURE 4
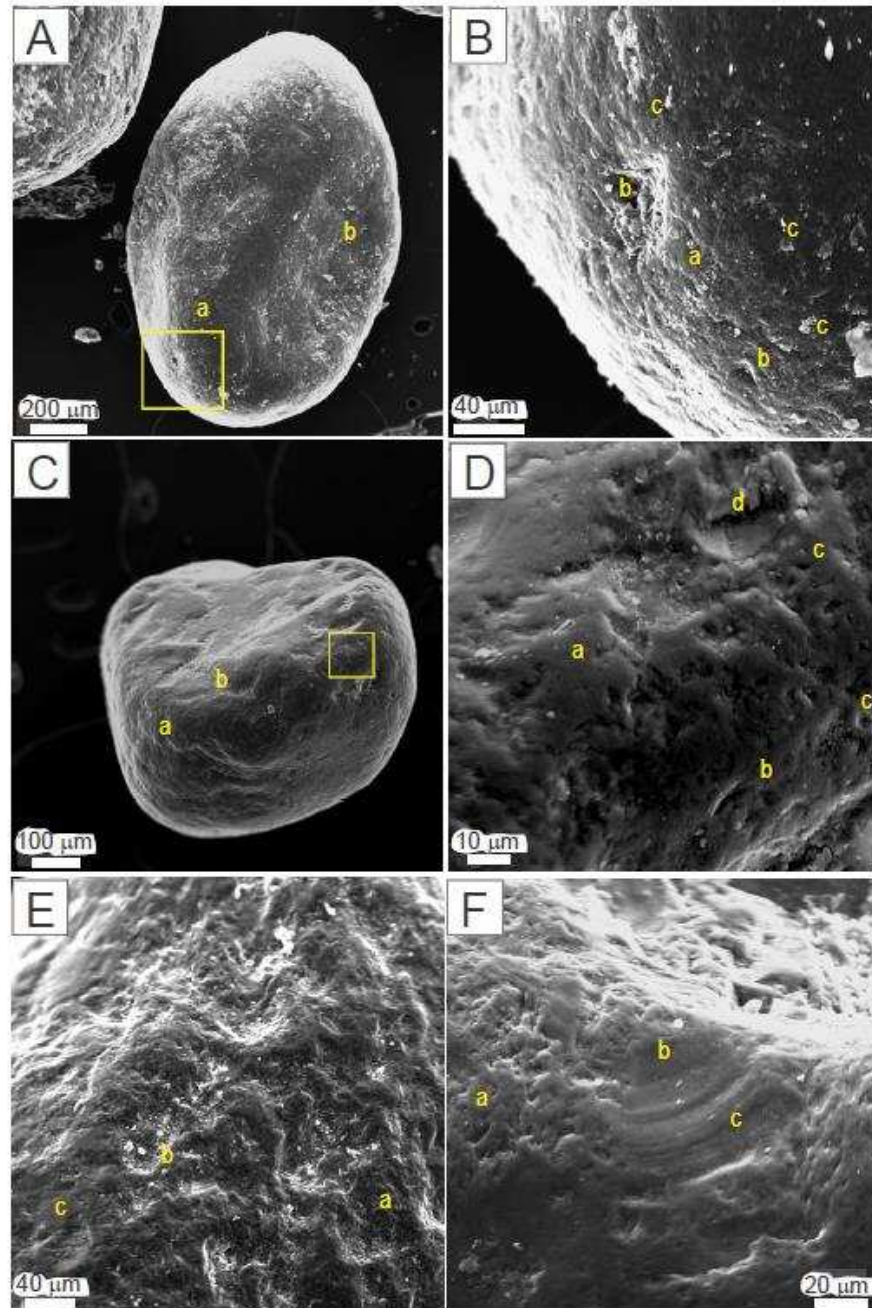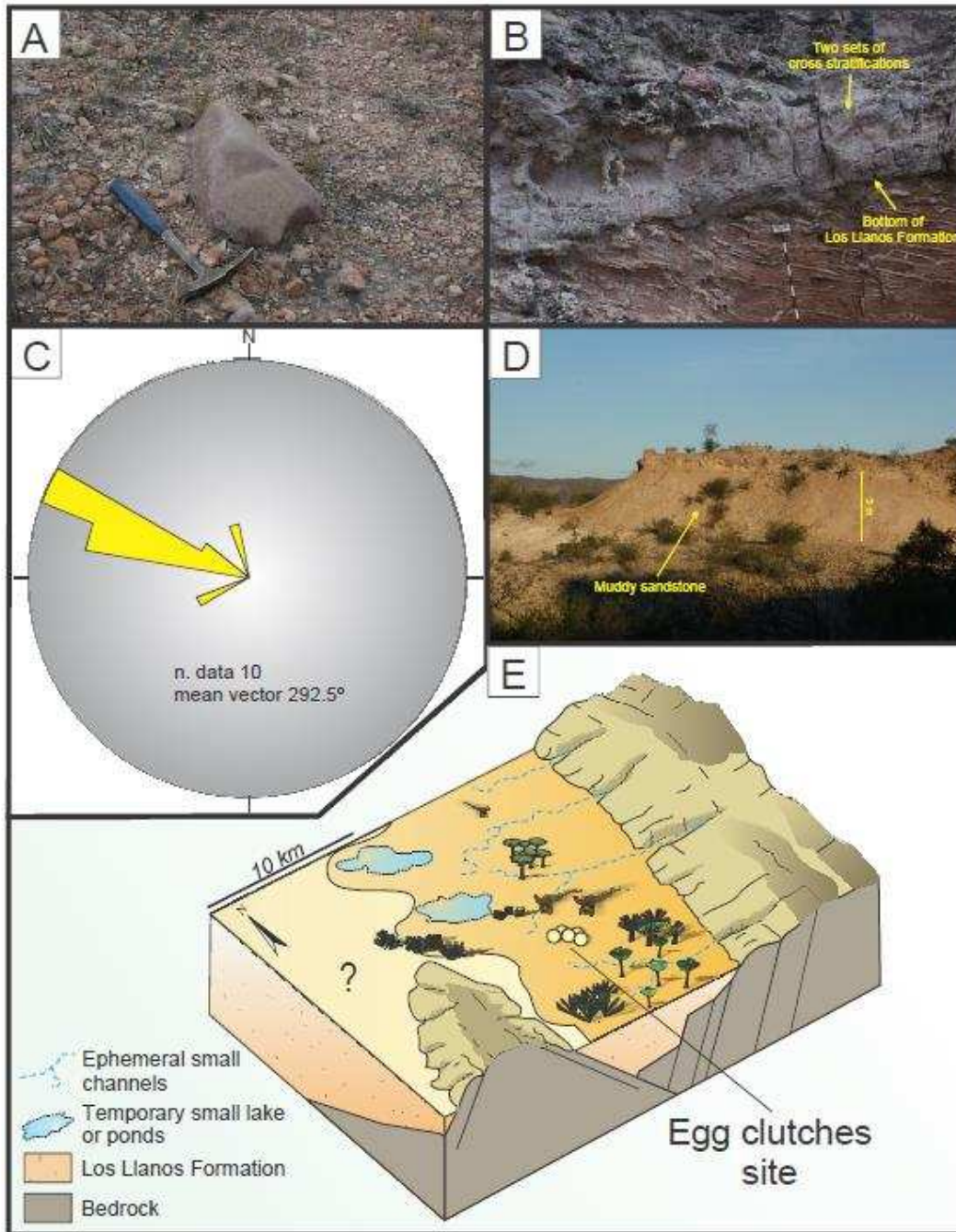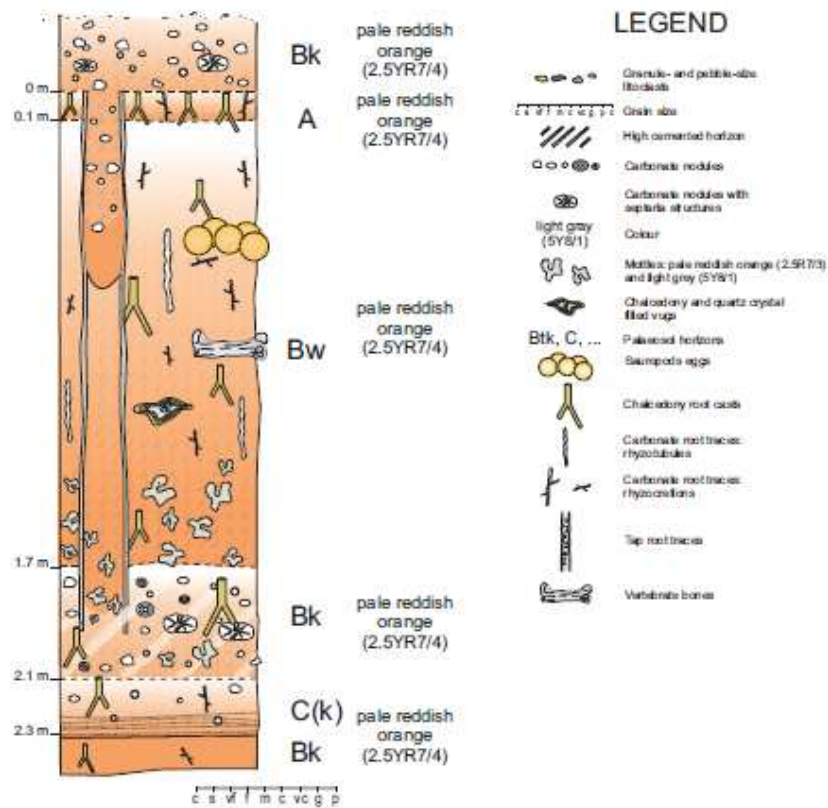
FIGURE 5

FIGURE 6

FIGURE 7
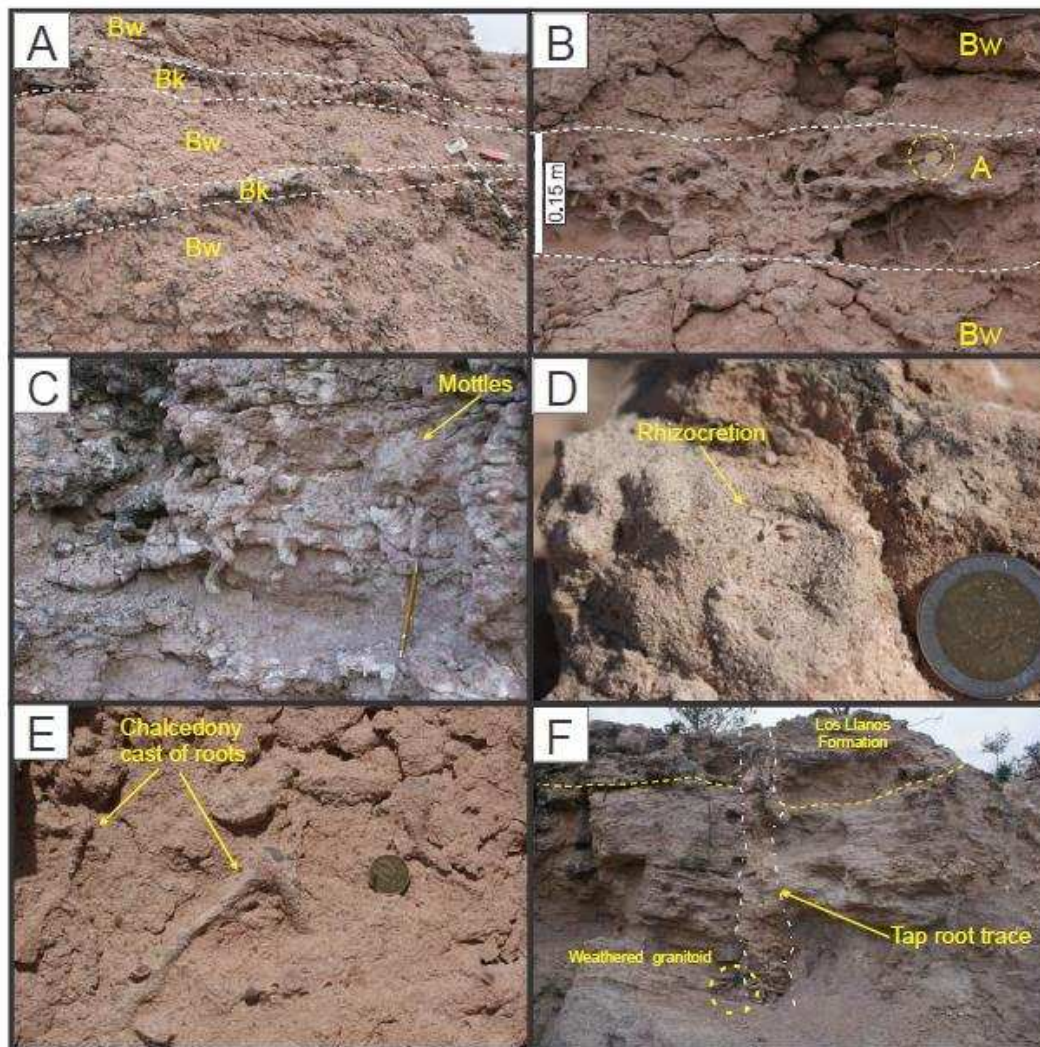
FIGURE 8
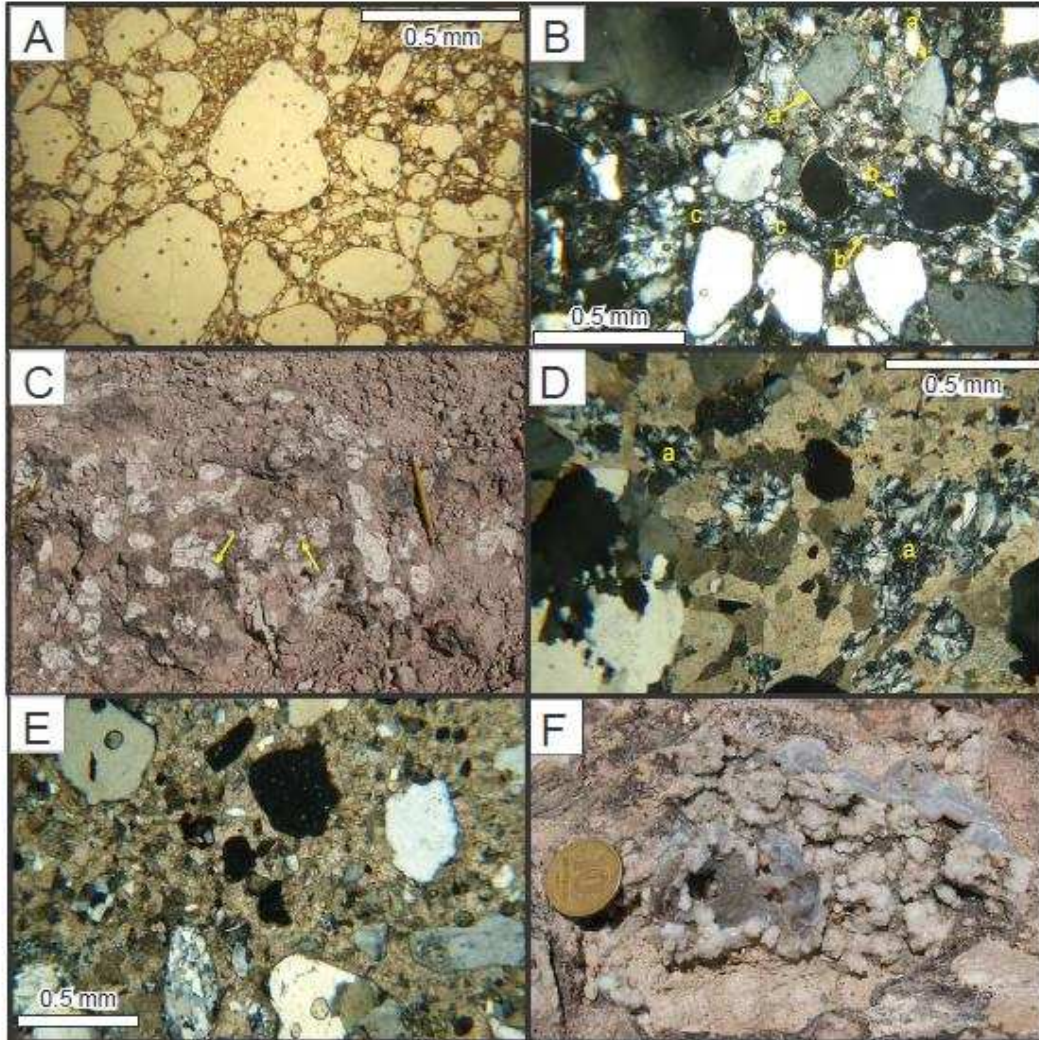
FIGURE 9
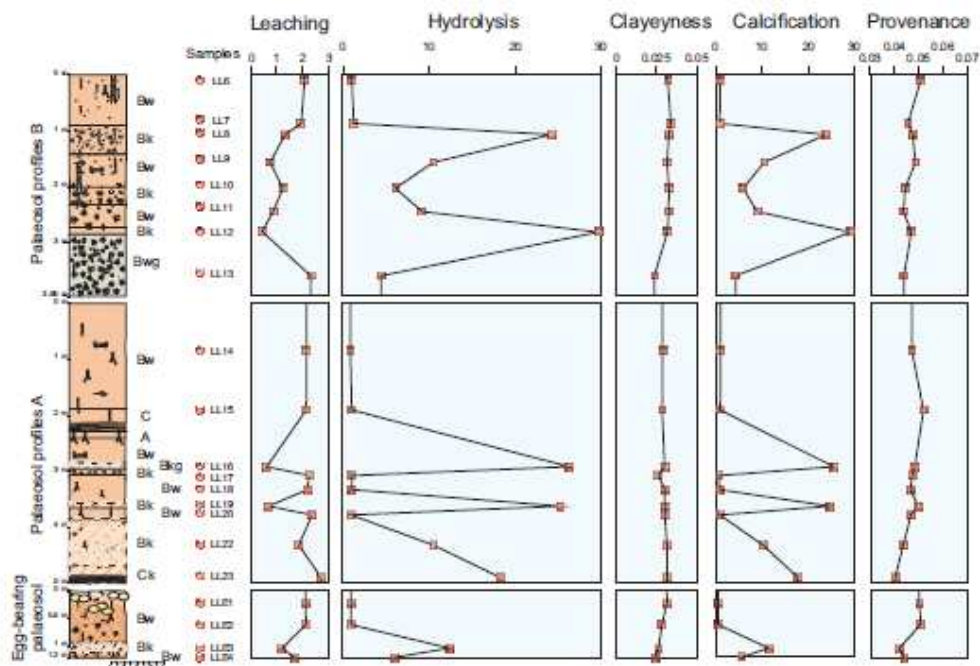
FIGURE 10
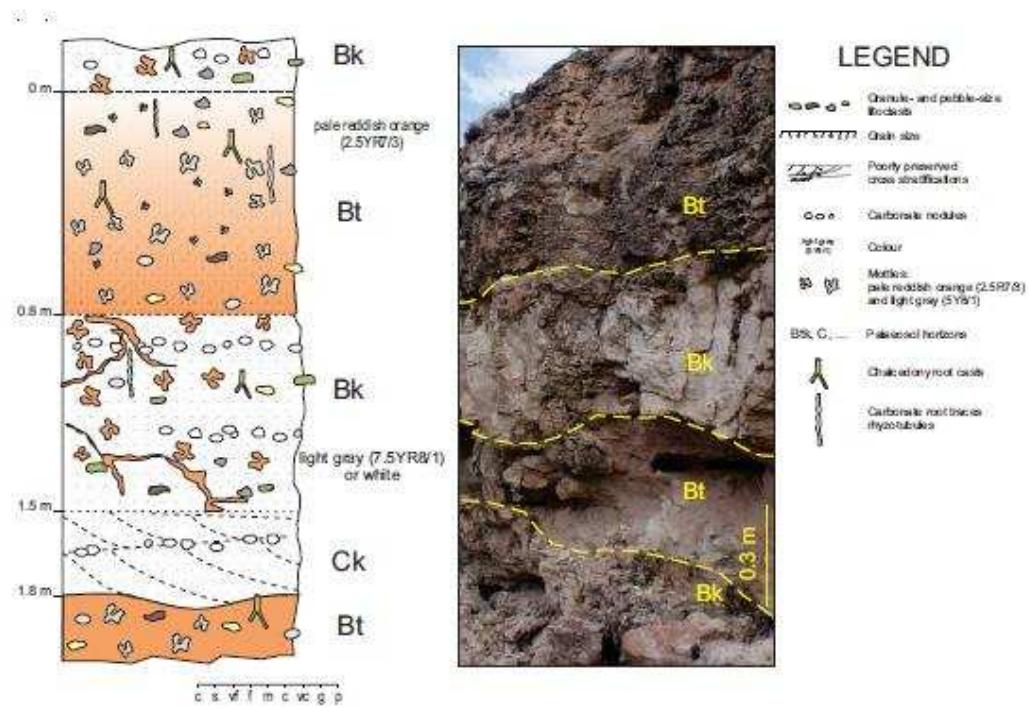
FIGURE 11
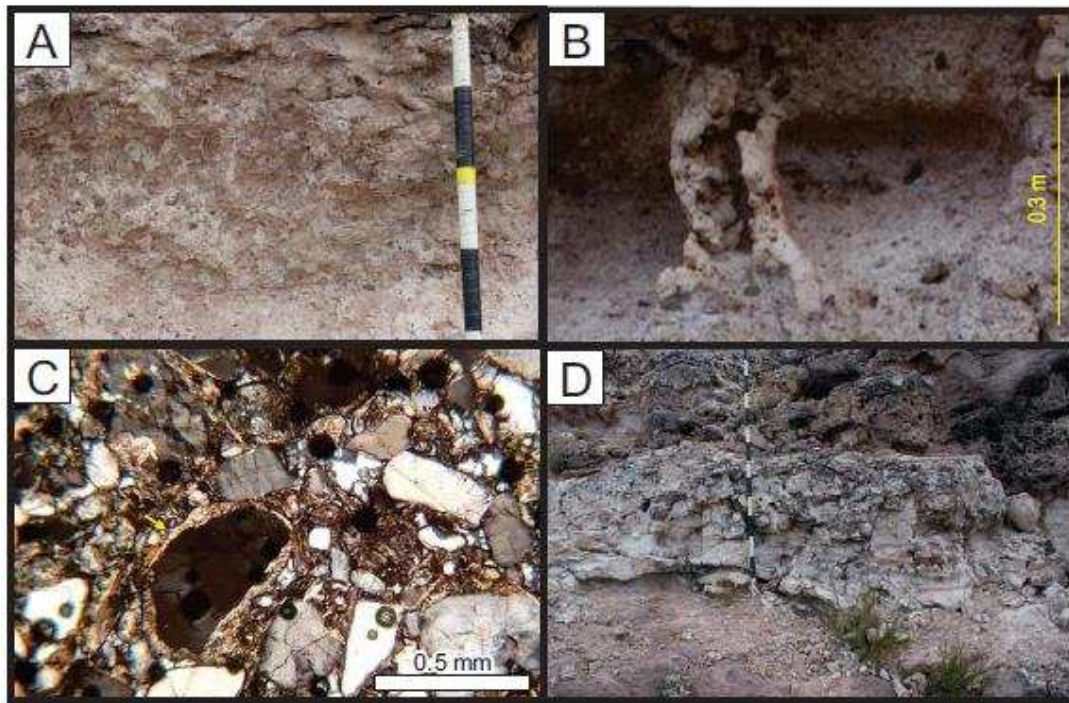
FIGURE 12
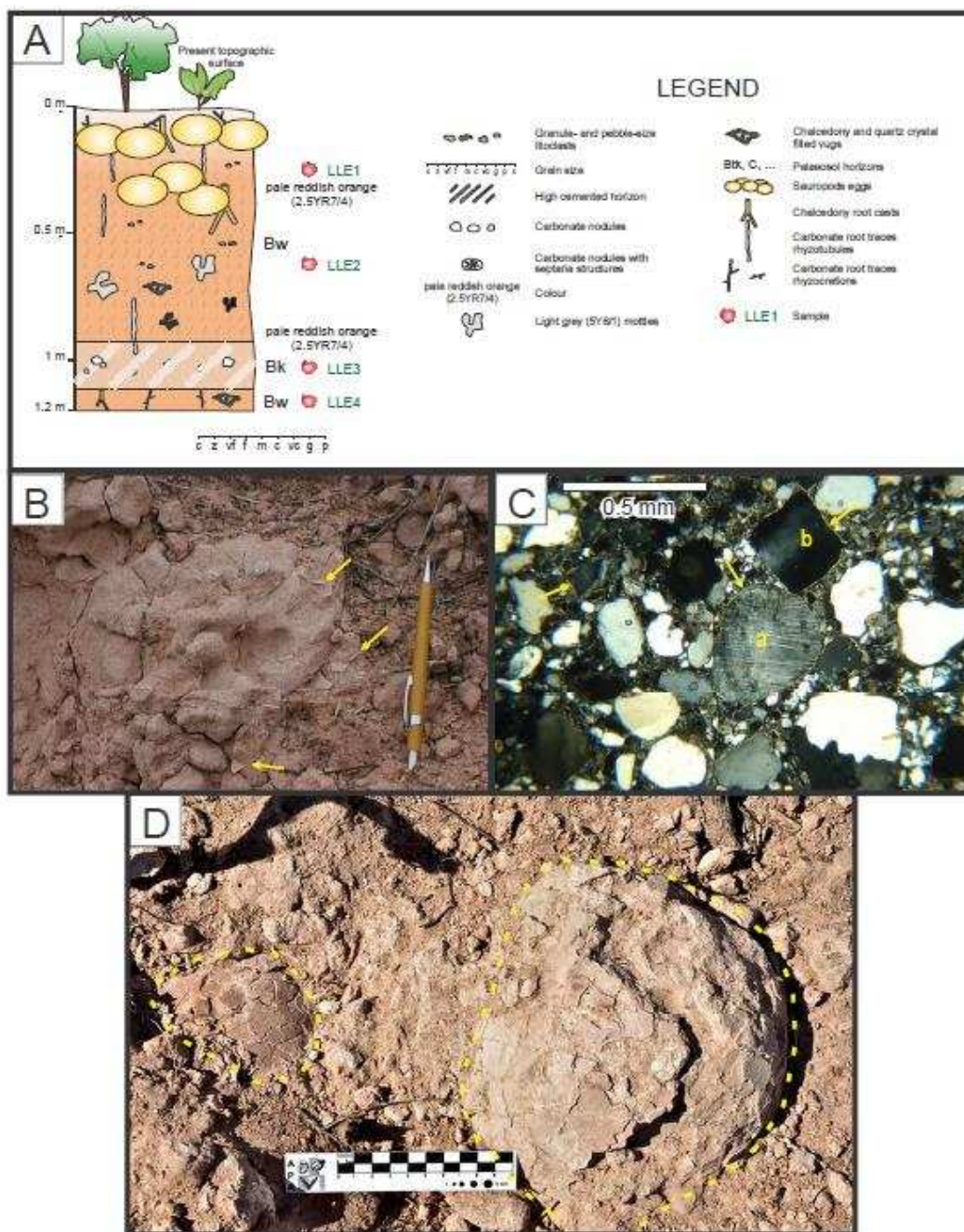
FIGURE 13
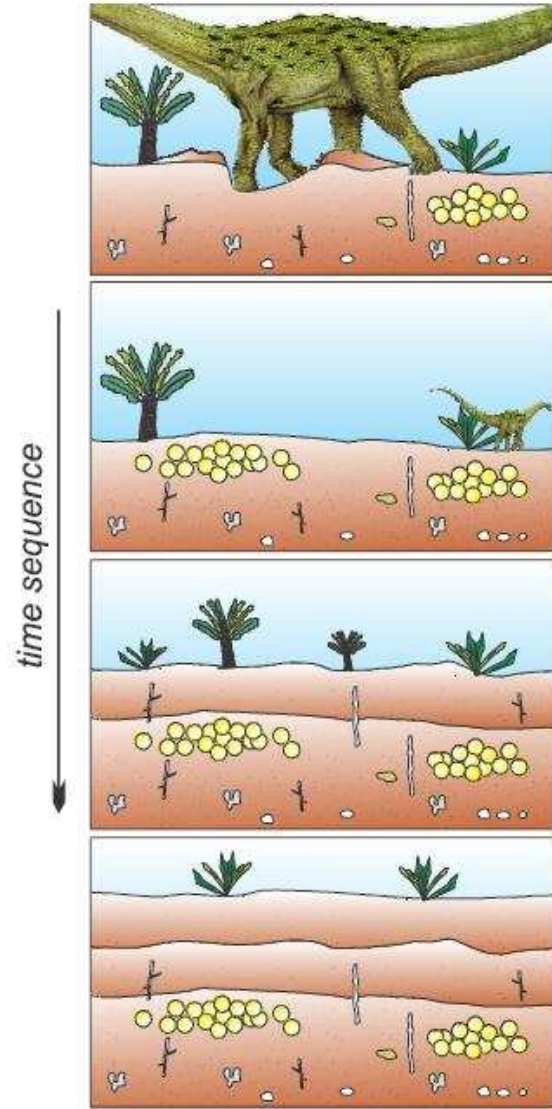
FIGURE 14
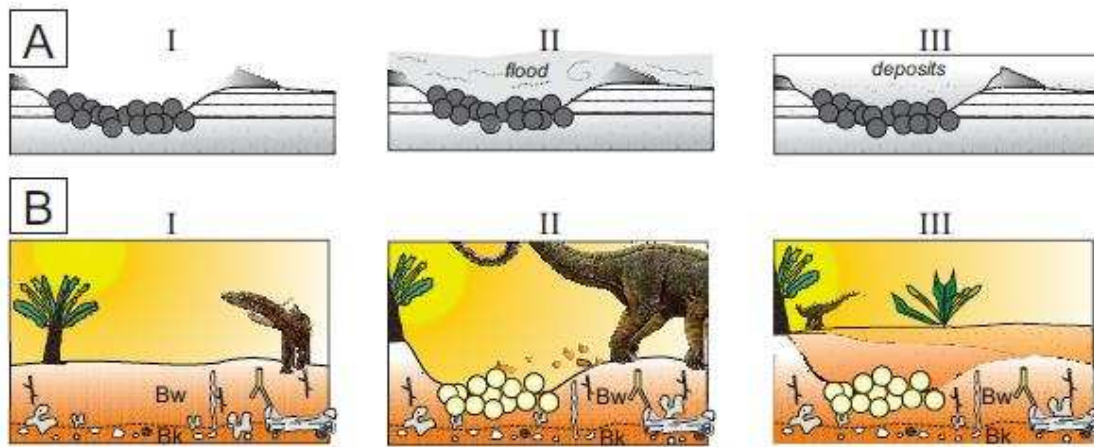
FIGURE 15

Graphical abstract
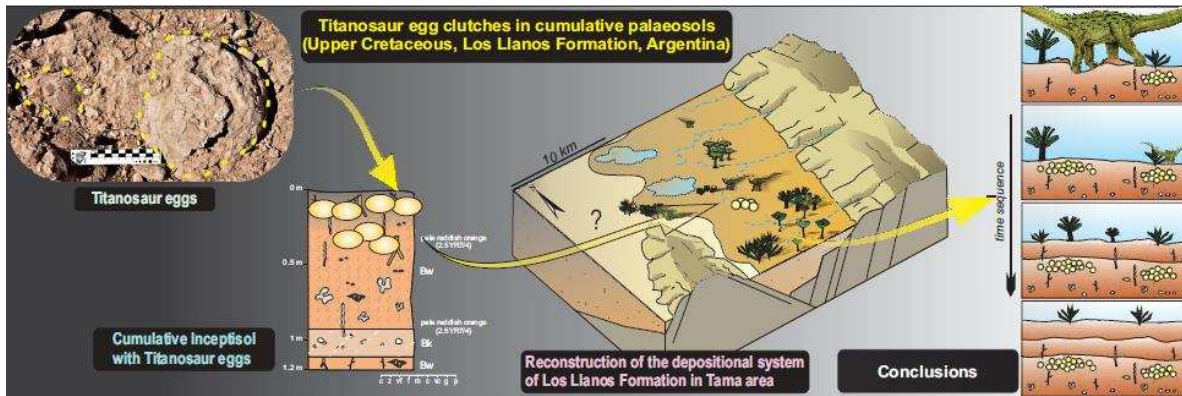
HIGHLIGHTS

- Cumulative palaeosol is optimal site to accumulate and preserve titanosaur clutches.

- This contribution helps to clarify the sites that titanosaurs selected to lay eggs.

- This study can contribute to the reconstruction of the palaeohabitat of titanosaurs.

- This study contributes to the study of nesting strategy of titanosaurs.